Dose Estimation for the European Epidemiological Study on Pediatric Computed Tomography (EPI-CT)

Authors: Thierry-Chef, Isabelle, Ferro, Gilles, Le Cornet, Lucian, Dabin, Jérémie, Istad, Tore S., et al.

Dose Estimation for the European Epidemiological Study on Pediatric Computed Tomography (EPI-CT)

Isabelle Thierry-Chef,[a,b,c,d,1] Gilles Ferro,[a] Lucian Le Cornet,[e,f] Jérémie Dabin,[g] Tore S. Istad,[h] Andreas Jahnen,[i] Choonsik Lee,[j] Carlo Maccia,[k] Françoise Malchair,[k,l] Hilde M. Olerud,[m] Richard W. Harbron,[b,c,d,n,o] Jordi Figuerola,[b,c,d] Johannes Hermen,[i] Monika Moissonnier,[a] Marie-Odile Bernier,[p] Magda Bosch de Basea,[b,c,d] Graham Byrnes,[a] Elisabeth Cardis,[b,c,d] Michael Hauptmann,[q,r] Neige Journy,[p,s] Ausrele Kesminiene,[a] Johanna M. Meulepas,[q] Roman Pokora[e] and Steven L. Simon[j]

[a] International Agency for Research on Cancer, Lyon, France; [b] Barcelona Institute for Global Health (ISGlobal), Barcelona, Spain; [c] Universitat Pompeu Fabra (UPF), Barcelona, Spain; [d] Ciber Epidemiología y Salud Pública (CIBERESP), Madrid, Spain; [e] Institute of Medical Biostatistics, Epidemiology and Informatics, University Medical Center Mainz, Mainz, Germany; [f] German Cancer Research Center, Heidelberg, Germany; [g] Belgian Nuclear Research Centre, SCK CEN, Mol, Belgium; [h] Norwegian Radiation and Nuclear Safety Authority, NO-0213 Oslo, Norway; [i] Luxembourg Institute of Science and Technology, Esch-sur-Alzette, Luxembourg; [j] Division of Cancer Epidemiology and Genetics, National Cancer Institute, National Institutes of Health, Rockville, Maryland; [k] CAATS, Sèvres, France; [l] ZEPHYRA, Liège, Belgium; [m] University of South-Eastern Norway, Faculty of Health and Social Sciences, Kongsberg, Norway; [n] Institute of Health and Society, Newcastle University (UNEW), Newcastle upon Tyne, United Kingdom; [o] NIHR Health Protection Research Unit in Chemical and Radiation Threats and Hazards, Newcastle University, United Kingdom; [p] Institut de Radioprotection et de Sûreté Nucléaire, Laboratoire d'épidémiologie des Rayonnements Ionisants, Fontenay-aux-Roses, France; [q] Department of Epidemiology and Biostatistics, Netherlands Cancer Institute, Amsterdam, the Netherlands; [r] Institute of BiostatisTics and Registry Research, Medical University Brandenburg Theodor Fontane, Neuruppin, Germany; and [s] French National Institute of Health and Medical Research (Inserm) Unit 1018, Centre for Research in Epidemiology and Population Health (CESP), Cancer and Radiations Group, Gustave Roussy, Villejuif, France

Thierry-Chef, I., Ferro, G., Le Cornet, L., Dabin, J., Istad, T. S., Jahnen, A., Lee, C., Maccia, C., Malchair, F., Olerud, H. M., Harbron, R. W., Figuerola, J., Hermen, J., Moissonnier, M., Bernier, M-O., Bosch de Basea, M., Byrnes, G., Cardis, E., Hauptmann, M., Journy, N., Kesminiene, A., Meulepas, J. M., Pokora, R. and Simon S. L. Dose Estimation for the European Epidemiological Study on Pediatric Computed Tomography (EPI-CT). *Radiat. Res*. 196, 74–99 (2021).

Within the European Epidemiological Study to Quantify Risks for Paediatric Computerized Tomography (EPI-CT study), a cohort was assembled comprising nearly one million children, adolescents and young adults who received over 1.4 million computed tomography (CT) examinations before 22 years of age in nine European countries from the late 1970s to 2014. Here we describe the methods used for, and the results of, organ dose estimations from CT scanning for the EPI-CT cohort members. Data on CT machine settings were obtained from national surveys, questionnaire data, and the Digital Imaging and Communications in Medicine (DICOM) headers of 437,249 individual CT scans. Exposure characteristics were reconstructed for patients within specific age groups who received scans of the same body region, based on categories of machines with common technology used over the time period in each of the 276 participating hospitals. A carefully designed method for assessing uncertainty combined with the National Cancer Institute Dosimetry System for CT (NCICT, a CT organ dose calculator), was employed to estimate absorbed dose to individual organs for each CT scan received. The two-dimensional Monte Carlo sampling method, which maintains a separation of shared and unshared error, allowed us to characterize uncertainty both on individual doses as well as for the entire cohort dose distribution. Provided here are summaries of estimated doses from CT imaging per scan and per examination, as well as the overall distribution of estimated doses in the cohort. Doses are provided for five selected tissues (active bone marrow, brain, eye lens, thyroid and female breasts), by body region (i.e., head, chest, abdomen/pelvis), patient age, and time period (1977–1990, 1991–2000, 2001–2014). Relatively high doses were received by the brain from head CTs in the early 1990s, with individual mean doses (mean of 200 simulated values) of up to 66 mGy per scan. Optimization strategies implemented since the late 1990s have resulted in an overall decrease in doses over time, especially at young ages. In chest CTs, active bone marrow doses dropped from over 15 mGy prior to 1991 to approximately 5 mGy per scan after 2001. Our findings illustrate patterns of age-specific doses and their temporal changes, and provide suitable dose estimates for radiation-induced risk estimation in epidemiological studies. © 2021 by Radiation Research Society

Editor's note. The online version of this article (DOI: https://doi.org/10.1667/RADE-20-00231.1) contains supplementary information that is available to all authorized users.

[1] Address for correspondence: Barcelona Biomedical Research Park (PRBB), Doctor Aiguader, 88, 08003 Barcelona, Spain; email: isabelle.thierrychef@isglobal.org.

INTRODUCTION

The use of computed tomography (CT) is widespread in most high- and middle-income countries around the world

(1, 2). While CT plays a crucial role in modern healthcare, its widespread use continues to raise questions about the magnitude of doses received and associated health risks (3–5). CT technology has evolved considerably since its introduction in the 1970s, resulting in faster data acquisition and better image quality for diagnostic medical purposes. CT doses, particularly to pediatric and adolescent patients, have been reduced, mostly since the early 2000s when attention was drawn to the inappropriate use of adult scan settings (6–8), particularly with the introduction of multi-slice CT scanners (9, 10).

Radiation protection standards continue to rely primarily on the analyses of the Life Span Study (LSS) cohort of atomic bomb (A-bomb) survivors (11–13), which includes subjects of all ages at time of exposure, who experienced full-body, near-instantaneous exposures to high-energy gamma rays and neutrons. This exposure situation is very different from the much-lower-energy partial-body fractionated exposures commonly received from medical diagnostic procedures (14–16). To elucidate the magnitude of the actual health risk associated with CT examinations in pediatric and adolescent patients, epidemiological and modeling investigations have been conducted (7, 17–29).

The European Epidemiological Study to Quantify Risks for Paediatric Computerized Tomography (EPI-CT study) (see http://epi-ct.iarc.fr/) was designed to overcome limitations of previously reported studies and increase the statistical power of direct estimates of the cancer risks from radiation doses associated with CT scanning in childhood and adolescence (30).

A major aspect of the study was the improvement of dose reconstruction. For this, we developed a comprehensive dose reconstruction strategy and a means to estimate uncertainty on an individual basis. This effort included collection of relevant dose-related data, recognizing the major difficulties arising from the very large scale and international nature of the data (30, 31), with an intent to provide the best basis for retrospective evaluation of the dose-response relationship. Data collected in the study are also a source of key information concerning past and current radiological practices and evolution of doses associated with pediatric CT scanning over time (32, 33).

Within EPI-CT, CT data were collected for a total of 948,174 pediatric patients[2] from Belgium, Denmark, France, Germany, the Netherlands, Norway, Spain, Sweden and UK. By definition, all patients have had at least one CT scan before the age of 22 between the late 1970s, when CT first became available, and 2014, the end of the study (31). The aim of this work is to present the methods used to estimate individual organ doses[3] and associated uncertainties for the entire cohort, as well as to summarize estimated

doses for this cohort, which, to our knowledge, represents the largest such dataset currently available.

MATERIALS AND METHODS

Data Collection

The EPI-CT cohort of 948,174 was constructed by extraction of archived patient information from the Radiology Information System (RIS) of radiology departments of the 276 participating hospitals from the nine participating countries (31). All personal data were de-identified to protect patient privacy and a unique pseudo-anonymized identification number was used at the international level. Data collection for dosimetry consisted primarily of the following: 1. Analyzing published national surveys; 2. Acquiring data on imaging protocols by questionnaire (see Supplementary Material; https://doi.org/10.1667/RADE-20-00231.1.S1); and 3. Data extraction from the RIS and Picture Archiving and Communication System (PACS).

Data on 1,430,454 examinations were extracted from the RIS of the participating hospitals. The RIS is devoted to administrative recording of the radiology department activities and includes personal identifiers, date of birth, date and type of CT examination (i.e., body region examined). Technical parameters, including scanner model, bowtie filter, tube potential, pitch and scan range, along with exposure indicators such as computed tomography dose index (CTDI) and dose length product (DLP), were not generally recorded in the RIS data. Other sources were used for these details (see below). Recording practices in the RIS differed substantially between time periods and departments. For example, a CT scan with and without the use of contrast media might be represented by one or two entries in the RIS, depending on institutional practices and time period. We describe methods to account for this and other uncertainties as an integral part of our dose assessment. We used a number of sources of data on technical scan parameters used for clinical CT scans. Wherever possible, information was obtained for specific scan types and sub-types (e.g., both routine head scans and head sub-regions such as pituitary fossa or internal auditory meatus) and patient age.

The primary source of technical information was metadata from a sample of images stored on PACS. PACS was introduced gradually in hospitals after the mid 1990s and is now widely employed in radiology departments. PACS allows systematic recording and archiving of all images together with associated machine settings recorded in the Digital Imaging and Communications in Medicine (DICOM) header of each image. The specialized PACS data extraction software packages, PerMoS (34) and Gladys (35), were used to extract technical parameters from data stored in these DICOM headers. For each CT image recorded in PACS, the software retrieved and extracted information on CT machine model, identification and characteristics of the patient (sex, date of birth), as well as data on the examination itself, including scan date, protocol name indicating body region scanned, and the machine settings selected for the examination (e.g., kV, mA, exposure time, etc.). We did, in the extraction algorithm, account for some missing parameters (e.g., calculation of a missing pitch based on table feed and total collimation) and vendor-specific information (e.g., specific code for exposure depending on manufacturer). To respect patient privacy/data governance requirements, the images themselves could not be gathered, only exposure metadata. Therefore, it was not possible to obtain patient measurements, e.g., torso thickness, etc. or determine scan range in relationship to patient anatomy. Information on height and weight of patients was not available in either RIS and PACS datasets. Our dose reconstruction is, therefore, based on patient age.

Data extracted from PACS for the same examinations could not be easily linked on a one-to-one basis with data recorded in RIS because of incompatibilities between the systems, as well as due to the mandatory anonymization process. Links between the systems for individuals were, unfortunately, often not kept at the hospital level. Consequently, the

---

[2] The EPI-CT study assembled data on patients below 22 years of age. They are referred to as pediatric patients throughout this article. The mean age at first scan for the full cohort is 10 years (31).

[3] Throughout this article, mean absorbed dose to specific organs is referred to as organ doses.
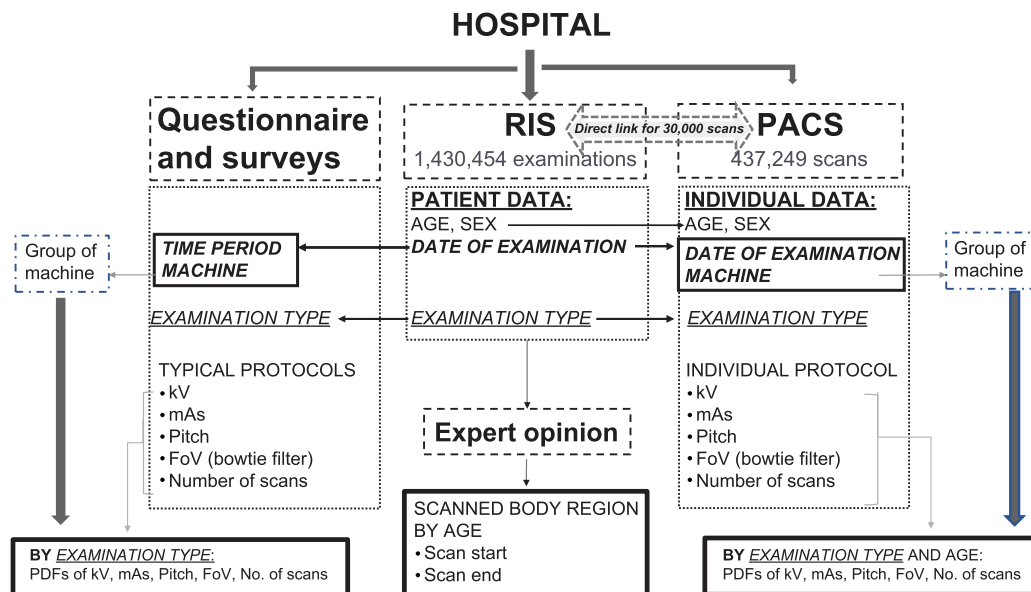
HOSPITAL

FIG. 1. Scheme of data availability and strategy for dose reconstruction. Sources of data are indicated in dotted boxes. Arrows indicate the link between data and provide the grouping strategy to derive PDFs of the main parameters of the protocols. For the 948,174 members of the EPI-CT cohort, a total of 1,430,454 CT examinations were extracted for the Radiology Information System (RIS). In parallel, technical information could be extracted from the Picture Archiving and Communication System (PACS) for 437,249 individual scans, of which only 30,000 could be identified in the RIS dataset.

PACS dataset was not used at the individual patient level but was the primary data source to generate the imaging protocols for a range of patient ages, CT machines, and associated time periods and types of examination. Linkage between PACS and RIS data was only possible for a relatively small subset of CT scans (30,000).

PACS data were only available for scans performed after 1995. For earlier scans, we obtained information on scan parameters from national surveys of CT practice in the UK (*36*) and Norway in the 1980s and early 1990s (*32, 37*). In addition, a questionnaire was sent to each participating radiology department to collect information required for dose reconstruction, in particular, machine type and associated imaging protocols used within defined time periods for common pediatric examinations (head, chest, abdomen/pelvis[4]) (See Appendix 1 in Supplementary Material; https://doi.org/10.1667/RADE-20-00231.1. S1). The parameters of primary interest were those necessary for dose calculation: peak tube potential (kV), the tube current-time product (mAs), choice of field of view (FoV) associated to bowtie filter, (head or body), and scanner pitch. The questionnaire requested the historical imaging protocols used for 5-year-old children, although detailed protocols for other age groups (or for different body weight groups) could also be included by the participating hospital.

Protocols derived from national surveys, questionnaire and PACS data were the initial steps to the dose-estimation strategy implemented in EPI-CT. The strategy and process to generate imaging protocols and estimate doses based on collected information is shown in Fig. 1.

NCICT Organ Dose Calculator

The National Cancer Institute Dosimetry System for CT (NCICT, a CT organ dose calculator), version 1.0 (*38–40*) (https://ncidose.cancer.

gov/#ncict), was selected as the most appropriate CT organ dose calculator (*41*). NCICT provides estimated organ doses from lookup tables of $CTDI_{vol}$[5]-to-organ dose conversion coefficients derived from Monte Carlo radiation transport calculations combined with a library of hybrid phantom models developed by the University of Florida/National Cancer Institute and the International Commission on Radiological Protection (ICRP) (*42, 43*). The use of these anatomically realistic phantom models gives NCICT an advantage over other lookup table-based dose calculators such as CT Expo (*44*) and ImPACT (*45*), which use simpler, mathematical phantoms based on the Oak Ridge National Laboratory (ORNL, Oak Ridge, TN) model (*46*). The validity of NCICT was determined by experimental measurements reported by Dabin *et al.* (*47*) using a physical phantom representing the body size of a 5-year-old child and five different scanner models [Siemens Somatom Emotion 6 and 128 row Definition Flash (Malvern, PA), Philips Brilliance 64 (Andover, MA), 80-slice Toshiba Aquilion Prime (Tustin, CA) and 64-slice GE LightSpeed VCT (Waukesha, WI). Variation in dose estimates between NCICT and experimental measurements were within $\pm 20\%$ for most organs.

If $CTDI_{vol}$ was not available, which was the case for the vast majority of examinations, NCICT estimated this figure based on the combination of kV and mAs using a scanner manufacturer and model-specific library of conversion coefficients (*39*). While the simulation library of NCICT was derived for one reference scanner (Siemens SOMATOM Sensation 16), the software takes advantage of the well-benchmarked assumption that organ doses estimated for one CT scanner can be converted into organ doses for another CT scanner using the ratio of the $CTDI_{vol}$ between the scanners (*38, 47–49*).

In the NCICT version available at the time of the project, the organ dose calculation was possible for 12 phantoms (females and males, each for six ages: newborn, 1-, 5-, 10-, 15-year-old and adult). Interpolations of phantoms based on typical height for a given age and sex (from 0 through 20 years, male and female) was performed to allow matching (to the nearest rounded year of age) between each

---

[4] The body region exposed in abdominal CTs included the pelvic region to be representative of the practice. However, pelvic examinations are still considered separately as they might be performed in specific conditions without any interest to the upper abdominal region.
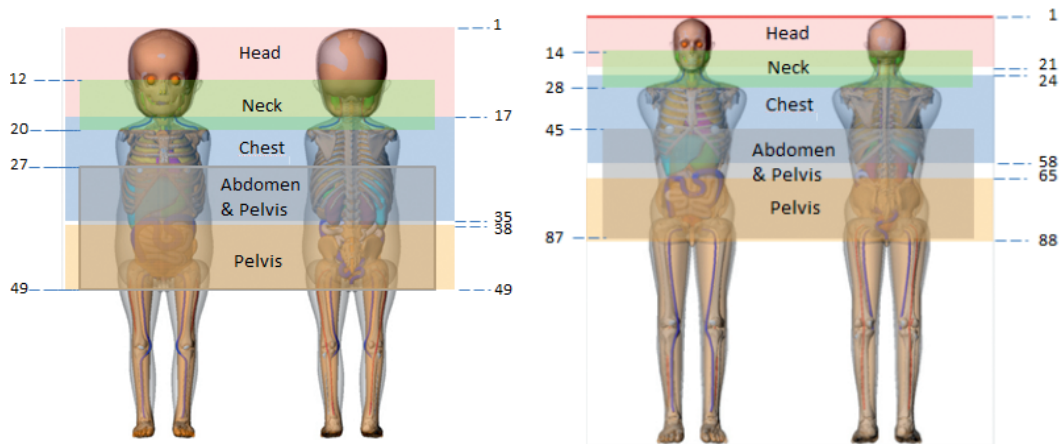
[5] CTDIvol: volume Computed Tomography Dose Index.

FIG. 2. Definition of scanned body regions with start and stop landmarks for the main examination types in two representative age groups: 1 year (left panel) and 15 years (right panel). Measurements are in cm, from the top of the head.

subject in EPI-CT cohort and the most representative phantom (age-specific phantom). Based on the 12 existing phantoms (six ages and two sexes), interpolation was made so that each 1-cm slice of the reference phantom has a corresponding slice in younger and older phantoms. Since information on patient height and weight was not usually recorded in the RIS or PACS databases, the selection of a specific phantom, based on patient age, was a surrogate of expected body size (where height and weight are recorded, these figures are often based simply on values stated by parents and are thus not particularly reliable). Potential error in dose estimation due to variations in human morphometry from the assumed body size (including variation in fat distribution and organ shape) was not included in the uncertainty analysis at this stage.

NCICT provides dose estimates as a function of the following input parameters: age and sex of the patient; body region scanned (identified by the scan start and stop landmarks measured in cm from the top of the head); scanner manufacturer and model; imaging protocol parameters with separate entries for kV, mAs, choice of field of view (FoV) associated to bowtie filter (head or body), and scanner pitch. NCICT does not incorporate gantry tilt; zero gantry tilt is, therefore, assumed for all scans.

Doses were estimated in this study using the NCICT for 33 organs and tissues. For space considerations, organs of high relevance in the context of childhood exposure are presented in the main text. Because children are generally more radiosensitive to induction of leukemia, thyroid, breast and brain cancer and frequently at higher risk of developing cognitive effects, thyroid nodules and cataracts (50, 51), we present dose estimates for active bone marrow, brain, eye lens, thyroid and female breasts. Doses to other organs are provided in the

Supplementary Material (Appendix 2; https://doi.org/10.1667/RADE-20-00231.1.S1).

In the NCICT, the arms and hands of phantoms are removed (Fig. 2) to realistically simulate the arms-raised posture in body CT scans. This does not appreciably affect estimation of doses to bone marrow since only a small fraction of active marrow in pediatric patients is found in the forearms or distal humerus and thus exposed in CT examinations of the elbow, wrist or hand. For completeness, however, we calculated bone marrow doses in upper limbs by substitution (for example, ankle doses were used to estimate marrow doses to the wrist), using the fractions of active marrow in the two anatomical zones under comparison. Complementary to Fig. 2 is Table 1, which presents the proportion of the total-body active marrow within the scan region specified by start and end points and by age (42). Note that the proportions of active marrow in the specified body regions sum to more than 100% because some of the scan ranges overlap.

Two-dimensional Monte Carlo (2DMC) Method for Dose Reconstruction, Error Propagation and Uncertainty Estimation

In this study, dose estimation and uncertainty estimation were intimately connected steps which are described in detail below. Here, we define uncertainty to be the lack of knowledge about the true dose though, as explained here, we evaluated uncertainty for the entire distribution of doses for the cohort as well as on the individual patient level.

Numerous parameters necessary for organ dose reconstruction (e.g., machine used, machine settings, the number of scans per examination, etc.) were missing for most patients. Our approach to dose estimation,

TABLE 1
Proportion (%) of Active Bone Marrow by Scanned Body Region and Six Age Categories (42)

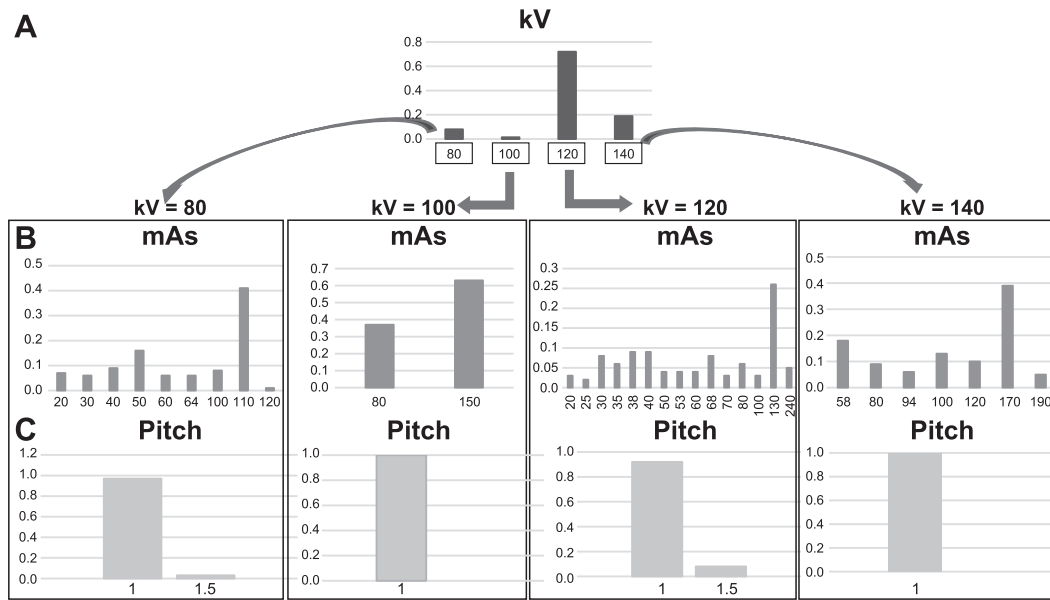| Age category	Head			Neck			Chest			Abdomen and pelvis		
	Scan Start (cm)	Scan Stop (cm)	%	Scan Start (cm)	Scan Stop (cm)	%	Scan Start (cm)	Scan Stop (cm)	%	Scan Start (cm)	Scan Stop (cm)	%
Newborn	1	12	28	8	14	16	11	25	31	18	35	27
1 year	1	17	34	9	20	15	17	35	32	27	49	32
5 year	1	20	35	9	23	14	20	43	27	33	62	33
10 year	1	20	19	9	24	9	22	49	36	38	76	47
15 year	1	21	12	11	28	7	24	58	35	45	87	60
Adult	1	23	5	11	28	5	24	60	40	46	93	64

FIG. 3. Diagram illustrating selection of parameter values by the 2DMC method. The PDFs represent the machine settings for Toshiba Aquilion 4/group 2 (multislice CTs with 2–4 slices) for chest examination of 5-year-old subjects (body FoV) after 2000. Row A: PDF for the tube voltage (kV). Row B: PDF for mAs. Row C: PDF for the pitch.

which inherently accounts for uncertainties due to missing and uncertain data, is the two-dimensional Monte Carlo (2DMC) simulation method (41, 52), accommodating varying degrees of availability and uncertainty of data, by country and time period.

The 2DMC method was designed to manage shared and unshared uncertainties and to produce sets of doses, each set called a realization and having a single estimate of dose to each organ for all cohort members. In the 2DMC method, uncertainty is represented not by deriving possible alternative doses on an individual subject basis but rather, by deriving alternative sets of doses for the entire cohort. This strategy correctly maintains inter-individual correlations because of exposure attributes shared among subgroups of patients (e.g., having been scanned in the same hospital). All realizations can be considered as a surrogate of true doses for the cohort, to evaluate and find the most significant dose-response relationship.

As noted, emphasis was on sampling parameters for the entire cohort, which maintains proper correlations among persons within subgroups who shared similar attributes. Each missing dosimetric parameter was derived from a probability density function (PDF) representative of the state of knowledge for the appropriate time period. The PDF for each missing parameter was built from the available data (obtained from PACS, surveys and questionnaire), based on thorough analysis of the data and appropriate grouping, as described in the sections below. A PDF provides the relative likelihood for any sampled value to equal the true value of the variable. For example, the distribution in each national cohort was used to derive the PDF to be used in case of missing information on sex. A typical PDF for sex is 0.56 male and 0.44 female (31). Following the PDF, a patient with unknown sex has a probability of 0.56 to be male and 0.44 to be female. Figure 3 provides another example of derived PDFs for parameters associated with the use of a given machine (Toshiba Aquilion), for chest CT on a 5-year-old child.

For each realization, a complete set of parameters was produced for all members of the entire cohort: Values of parameters shared among members of a subgroup (for example, the CT machine in use in a given hospital for a given time period) were sampled once from the appropriate PDFs for the entire subgroup, while unshared dosimetric parameters (for example, anatomical area explored) were sampled from the relevant PDFs on an individual basis for each CT scan. This sampling scheme maintains proper inter-individual correlations (Table 2) and is the basis of the 2DMC method.

The implementation of the 2DMC method in the EPI-CT study generated 200 realizations of the input parameters to be used to estimate 200 realizations of doses using NCICT. Each realization contains a single set of parameters for each of the 1.4 million examinations under investigation in EPI-CT, as well as the doses estimated for 33 organs using on NCICT (38) based on that set of parameters. The sections below provide a description of the sources of uncertainty and the methodology for producing PDFs for the various parameters sampled in the 2DMC modeling process (52).

Examination Type and Exposed Body Region

Examination names referring to body regions recorded in RIS and PACS were assigned using a hierarchical classification system of common CT radiological procedures and scanned body regions, as defined by the EU "Dose Datamed" projects (53, 54) (see Table 3), with head CTs, for example, divided into "skull and facial bones", "brain" and "head soft tissues", with finer descriptions in each category (orbits and petrous bones belonging to "skull and facial bones"). A PDF of exposed body regions was generated for each hospital for sampling by the 2DMC in each realization. This was used when data on examination type were missing or not classifiable.

For each body region in the classification (scan type and sub-type), scan start and end positions were assigned to the phantoms in the NCICT dose calculator. A correct assignment is important because the defined body region directly affects the portion of a given organ, and sometimes an entire organ, that is assumed to have been exposed. To assist in this determination, a panel of eight pediatric radiologists and radiographers from six European countries individually assessed typically used anatomical landmarks as start and end points to determine the body regions of interest for each of the 91 anatomical zones considered and the six reference ages. Anatomical regions from these six ages were then manually rescaled onto each of the age-specific male and female phantoms.

TABLE 2
Characteristics of Main Sources of Uncertainties and Methodology Applied within the 2DMC

Missing parameter	Strategy	Shared/unshared
Patient data		
Sex	PDF derived from National distribution	Unshared
Examination type	PDF derived from distribution at the level of hospital	Unshared
Exposed body region	Typical start and stop landmarks by examination type/body region and age (expert judgement) ± 1 cm	Shared + individual variability
CT machine		
No. of CT rooms in a given hospital	PDF derived from international distribution of number of rooms per hospital for two time periods (pre- and post-2001)	Shared
Machine (manufacturer and model)	PDF derived from national (or international) distribution of machine used in any given year	Shared
Remaining years of use	PDF derived from international distribution of number of remaining years of usage for two time periods (pre- and post-2001)	Shared
Protocols		
kV	PDF derived by group of machine, examination type/body region (and age in later years)	Shared
mAs	PDF derived by group of machine, examination type/body region, age (in later years) and kV	Shared
Pitch	PDF derived by group of machine, examination type/body region, age (in later years) and kV	Shared
FoV (bowtie filter)	16-cm head filter assigned to all head scans and 32-cm body filter assigned to all body scans except for newborns, where a 50% chance of use of the 16-cm considered for all body regions and 100% considered for head and neck	Shared
No. of scans	PDF of ''number of scans per examination'', specified by body region: 60 to 90% for single scan, 15 to 25% for two scans and 2 to 15% for more than two. If one or two entries in RIS for the same patient, body part and day, a maximum of four scans per examination allowed. If more than two entries in RIS, up to 10 scans per examination	Unshared

From the review with two medical physicists,[6] the scan start and end anatomical landmarks were refined to account for the following: 1. The fact that CT radiographers tend to increase the scan length to ensure that the radiologists are provided with the image they need for appropriate diagnosis; and 2. Over-scanning in helical CT (one additional helix performed automatically for image reconstruction). We therefore assumed a typical scanned region of the body to be equal to the maximum length derived by the panel of radiologists and radiographers (i.e., from the minimum start to the maximum end position), allowing for random variation of a maximum of ± 1 cm (with equal probability of values) on both ends of the scan (start and end) to account for the variability among patients, examinations and radiographers. Figure 2 shows, as examples, the typical start and end landmarks for head, neck, chest, abdominal/pelvic examinations for a 1-year-old child and a 15-year-old adolescent.

Machine Types and Associated Protocols

CT machines. The manufacturer and model of the CT machine used to perform each specific examination is well documented in the PACS dataset. This information was used to complement the information collected from hospital questionnaires or national surveys. When several machines were reported for a given hospital and time period, it was assumed that several CT rooms were available. We then considered that patients with examinations reported in the RIS could be scanned with equal probability with any of the available machines.

When no information on machine type used in a specific hospital for a given time period was available in either the questionnaire/surveys or PACS data, the distribution of machine types used in other

hospitals in the same country (or in the absence of national data, the international distribution) and in the same time period was used to construct a PDF from which the machine type was sampled.

In the case of missing information on machine type, the number of CT machines available in the hospital, equivalent to the number of CT rooms, was also unknown. For smaller hospitals, scanning less than 400 pediatric patients in a single year, we assumed that only a single CT machine was available. For larger hospitals scanning more than 400 patients in any given year, we sampled the number of CT rooms, allowing for up to three CT rooms per hospital prior to 2001 and up to six CT rooms in subsequent years. The selection of the number of rooms was based on a PDF of the number of CT rooms per hospital derived from PACS and questionnaire data.

When the duration of usage of a CT machine in a particular hospital was unknown, we estimated a period of use for that machine based on available data on duration of use of machines in all participating hospitals and countries. Prior to 2001, the remaining time of use of a CT machine could vary in the Monte Carlo sampling from one year to 15 years (at very low probability for these two extreme cases) with a maximum probability for usage time of 10 years. After 2001, the remaining time of use had a maximum of 11 years and a high probability around four years.

To generate PDFs for imaging protocols, we grouped the CT machines reported to have been used in participating hospitals into eight categories based on the number of slices imaged per rotation. The number of slices increased with time and represents the evolution in CT imaging technology. The first category included specific models of single-slice CT scanners which were used exclusively prior to 2001 and for which we found no evidence of use after 2001 in the PACS dataset (i.e., no protocol data for those models were available in the PACS dataset). Other models of single-slice CT scanners (used before and/or after 2001 with some data represented in the PACS dataset) were grouped together and the subsequent generations of CT machines were grouped as follows: 2–4 slices; 8–10, 16, 32, 64 and >64. The strategy we implemented for dose estimation, as discussed in the next section, was based on the assumption of a continuous introduction of

---

[6] Regular meetings and discussions between Isabelle Thierry-Chef, Steven L. Simon and the medical physicists (Carlo Maccia and Françoise Malchair) were organized to review both the set of collected data and derived PDFs for interpretation based on their long-standing experience in quality control and calibration of diagnostic imaging modalities in many different hospitals in Europe.

TABLE 3
Classification of CT Examinations based on EU Report RP154 (*53*)

Region of body		Part of Body		Specific exams and organs	
Code	Name	Code	Name	Code	Name
1	Head	11	Skull and facial bones	111	Skull
				112	Orbits
				113	Temporal bone/petrous bone
				114	Temporal-mandibular joint
				115	Sella turcica
				116	Face
				117	Dental
		12	Brain	121	Brain
				122	Cerebrum
				123	Posterior fossa
				124	Brain vascular
				125	Pituitary gland
		13	Head soft tissues	131	Sinus
				132	Internal auditory meatus
				133	Nasal cavity
				134	Mouth
2	Neck	21	Cervical spine	211	Cervical spine
		22	Neck	221	Larynx
				222	Pharynx
				223	Neck vascular
3	Chest	31	Thoracic spine	311	Thoracic spine
		32	Chest/thorax	321	Mediastinum
				322	Heart
				323	Thoracic aorta
				324	Lungs standard
				325	Lungs high resolution
				326	Lungs low dose
				327	Lungs vascular
4	Abdomen	41	Lumbar spine	411	Lumbar spine
		42	Abdomen	421	Full abdomen
				422	Upper abdomen
		43	Liver, pancreas and kidneys	431	Liver/pancreas
				432	Kidneys/Supra-renal glands
5	Pelvis	51	Pelvic bones	511	Hip/pelvic bone
				512	Sacrum/coccyx
				513	Sacro-iliac joint
		52	Pelvimetry	521	Pelvimetry (obstetric)
		53	Pelvis	531	Pelvis (soft tissues/vascular)
6	Limbs	61	Limbs	611	Shoulder
				612	Arm
				613	Elbow
				614	Wrist
				615	Hand
				616	Leg
				617	Thigh
				618	Knee
				619	Lower leg
				620	Calcaneum
				621	Ankle
				622	Foot
				623	Several limbs
7	Multiple regions	71	Head + neck	711	Supra-aortic trunks
		72	Neck + chest	721	Clavicle/collarbone
		73	Neck + chest + abdomen	731	Whole spine
		74	Neck to pelvis		
		75	Chest + abdomen	751	Thoracic lumbar spine
		76	Chest + abdomen + pelvis		
		77	Abdomen + pelvis	771	Uroscan
		78	Whole body	781	Head to thorax
				782	Head to abdomen
				783	Head to pelvis
		79	Other combinations		
8	Not classifiable				
9	Missing values				

TABLE 4
Summary Information on Data Collected for Dose Reconstruction (in Numbers)

Country	RIS data					PACS data		
	Hospitals	Patients	Examinations[a]	Questionnaire type data[b]	Period	Hospitals	Individual scans	Period
Belgium	2	10,074	14,204	7[c]	2001–2012	2	9,708	2001–2014
Denmark	6	17,696	33,006	0	1999–2013	1	3,755	2006–2012
France	23	119,399	171,696	23	2000–2011	10	12,143	2004–2014
Germany	20	47,096	71,559	3	1983–2010	19	73,584	1996–2013
Netherlands	43	148,135	217,799	3	1979–2014	22	104,594	1995–2010
Norway	27	77,252	139,563	45[3]	1980–2012	15	93,227	2001–2014
Spain	35	84,592	121,113	12	1991–2013	9	115,264	2000–2015
Sweden	28	121,805	185,460	20	1977–2013	1	16,835	1999–2011
UK	91	322,125	476,054	72	1985–2013	3	8,139	2000–2013
Total	276	948,174	1,430,454	185	1977–2014	63	437,249	1995–2014

[a] It should be noted that an examination may consist of one or more scans.

[b] Number of hospitals providing "questionnaire" type data (i.e., any type of information provided for a given hospital, mainly information on the machine type used was available).

[c] Includes data from non-participating hospitals.

new technology over time rather than on specific time periods for each type of machine with explicit cut-off dates for their use.

Imaging protocols and CT machine settings. An imaging protocol is a set of machine exposure settings selected by the radiographers performing each CT examination. The PDFs of machine settings from which values are sampled in the 2DMC process were derived using data collected through the national surveys and from the 437,249 individual scans recorded in the PACS (Table 4). The PDFs for each machine setting were generated based on: 1. the category of machine types, as discussed above; 2. the categories of examination: Head and neck, chest, abdomen/pelvis, pelvis, limbs and scans of multiple body parts; and 3. six age groups: Newborn (0–3 months), 1 year (4–30 months), 5 years (31–90 months), 10 years (91–150 months), 15 years (151–210 months), and adult (>210 months).

Imaging protocols obtained from pre-existing national surveys were used to generate PDFs of machine settings for the first category of machines (used exclusively prior to 2001). Norwegian protocols based on data collected in 1993 (*32, 37*) were combined with information obtained in the UK in 1989 (*36*). For the more recent time periods, imaging protocols were derived from the PACS dataset.

Imaging protocols were generated, by examination type, for the machine used in a given hospital/CT room with an additional distinction made by time period: 1. years when identical values of kV, mAs and pitch were used for all patients being scanned (i.e., similar protocols were used for adults and children); and 2. years when identical values of kV, mAs and pitch were used for all patients within each age category, effectively representing the introduction of age-specific protocols. Based on expertise and a recently published evaluation by Lee *et al*. (*55*), the introduction of pediatric (age-specific) protocols was simulated in our analysis by a step-wise increase in the proportion of hospitals having begun using pediatric protocols and automatic exposure control (*56, 57*). The step-wise increase was assumed to become effective after 1995 and was modeled as a 5% increase in 1996, 10% in 1997, then increasing by 10% per year to 90% in 2005, and tapering to 95% in 2006 and afterward. In this process, 2001 was the year we assumed that one half of the hospitals had introduced pediatric protocols (*58*).

Imaging protocols were applied to individuals according to examination type and age (after a given date, as described above), for the machine used in the corresponding hospital room at a specific time period. For each of the 200 realizations of the dose, the parameters of kV, mAs, pitch and choice of one of the two types of bowtie filter (head or body) were sampled from the appropriate PDF, according to machine category (Fig. 3). In the sampling process of the 2DMC, the value of kV was selected first and values for mAs and pitch were selected as a function of the kV to ensure that appropriate

correlations were maintained. In the absence of any information on the dimension of the bowtie filter used to shape the X-ray beam, we assigned the filter matching a 16-cm-head phantom for all head examinations and the filter matching a 32-cm-body phantom for body examinations. For newborns, recommendations were to use the 16-cm-filter irrespective of the examined body region. However, this practice was not always followed at the participating hospitals and a 50% chance of use of the 16-cm filter was, therefore, assumed for all body regions except head and neck (where 100% was assumed).

Scan vs. Examination of A Given Body Region

This study differentiated between scans and examinations: a scan is defined as a single pass through the CT machine. In contrast, an examination may consist of one or more scans, e.g., when images are needed before and after contrast media injection.

For the vast majority (94%) of data recorded in RIS, there was only one entry in RIS for the same patient, the same body region and the same examination date. However, approximately 5.5% of the records included two entries, with the same body region examined on the same day and 0.5% had more than two identical entries. The latter situation with more than two entries could be due to several possible scenarios: 1. CT examinations comprising multiple scan phases, e.g., pre- and post-contrast agent administration; 2. recording of additional post-CT reconstructions with no additional dose; 3. Non-radiation events such as administration of sedation or contrast media; or 4. Recording errors. The percentage of multiple entries for a given body region per day varied widely by hospital and year. Contact was made with local radiographers to investigate whether the recorded scans were real or artefactual, with particular attention on hospitals with much higher average number of multiple entries per day than elsewhere. The information obtained was discussed by a task group of dosimetrists and medical physicists and led to the implementation of a strategy to account for the possibility of multiple scans per examination within the uncertainty component of the dose estimation. Identified duplicates were removed from the dataset and remaining entries in the RIS were all assumed to be performed as a single scan. Total dose for each examination (dose per examination) was estimated as the dose for one single scan (dose per scan) multiplied by a factor to account for uncertainties on both: 1. multiple scans per examination (for example use of contrast media in a second scan); and 2. multiple examinations on the same day [Eq. (1)].

$$(D_{T,E})_i = (D_{T,S})_i * x_i, \tag{1}$$

where: $(D_{T,E})_i$ is the absorbed dose (mGy) to a tissue or organ per examination in a given realization; $(D_{T,S})_i$ is the absorbed dose (mGy)

to a tissue or organ per scan per realization; and x_i is a random variable representing the number of scans (per examination or in total for multiple examinations on the same day).

For each realization of dose calculation [see Eq. (1)], the number of scans per examination was sampled from the related PDF. The PDFs of ''number of scans per examination'' were specified, by body region, as reported by Olerud *et al.* (*32*) for the early years and derived from the PACS dataset for more recent time periods (noting that the number of scans per examination in the Norwegian PACS dataset is comparable to the number in the international PACS dataset). In both time periods, 60 to 90% of the examinations were performed with a single scan, depending on the body part under investigation. Two scans per examination represented 15–25% of the examinations in the PACS dataset, and the remaining examinations with more than two scans represented between 2% to 15% of the examinations. When there were either one or two entries in RIS for the same patient, body part and day, a maximum of four scans was allowed in the sampling. In contrast, when there were more than two entries in RIS for the same body part performed in one day, up to 10 scans were allowed in the simulation, for the more recent time periods, as found in the PACS dataset (PDFs of the number of scans per examination for main examination types are provided in Appendix 3, Supplementary Material; https://doi.org/10.1667/RADE-20-00231.1.S1).

A useful dose metric for presentation purposes is the mean dose in organ T per scan averaged over all realizations, i.e., the arithmetic average of the n alternative values of dose ($n = 200$ realizations) for a single scan [Eq. (2)] produced using the 2DMC methodology (*52*).

$$\overline{D}_{T,S} \ = \ \frac{1}{n}\sum_{i=1}^{n}(D_{T,S})_i, \qquad (2)$$

where $\overline{D}_{T,S}$ is the arithmetic average over n realizations of absorbed dose (mGy) to a tissue or organ per scan, and $(D_{T,S})_i$ is the absorbed dose (mGy) to a tissue or organ per scan for each realization (i).

The mean organ dose per examination for each subject was also determined [see Eq. (3)], accounting for multiple scans per examination by sampling from the time-specific x_i distributions.

$$\overline{D}_{T,E} \ = \ \frac{1}{n}\sum_{i=1}^{n}(D_{T,S})_i * x_i, \qquad (3)$$

where $\overline{D}_{T,E}$ is the arithmetic average over n realizations of absorbed dose (mGy) to a tissue or organ per examination, and $(D_{T,E})_i$ is the absorbed dose (mGy) to a tissue or organ per examination for each realization (i) with x_i being the random variable representing the number of scans (per examination or in total for multiple examinations).

Validation of the Method and Doses

A number of important validation methods were designed and implemented to ensure reliability of dose estimation in the EPI-CT study. As noted, PDFs of protocols were derived from data abstracted mainly from the PACS database and national surveys. The process of combining the range of abstracted X-ray machine settings to define protocols could sometimes lead to combinations of parameters that are unsuitable or unlikely. A thorough review of all the X-ray machine parameter combinations that were part of defined protocols was conducted. This process led to the removal of some combinations of parameters that were unlikely to ever be used together and might, therefore, result in unrealistically small or large doses. In addition, we also performed dose range checking (i.e., a manual or automatic search of doses less than, or greater than established norms), with assistance from graphical analysis of simulation results. These were useful to identify unrealistic calculation results which were removed by prohibiting the code from allowing those imaging parameters to be combined together into a protocol.

Dose estimates were also validated through the following: 1. An internal comparison between doses estimated using the 2DMC methods described above and those estimated using detailed procedure-specific exposure data recorded in PACS; and 2. External comparison with previously published figures.

RESULTS

Table 4 provides a summary of data collected and used for dose reconstruction. The participation rate to the questionnaire survey was low (21%), mainly providing information on CT manufacturer and models used (94% of the completed questionnaires), referring to recent time periods even though the main objective was to obtain information on past practice. Only 23% of the participating hospitals provided information on machine settings, which were mostly limited to protocol for one of the main examination types (head, chest, abdomen/pelvis or others) and one age group. More informative than information collected via questionnaire, were the published results from national surveys and the detailed individual PACS data for 437,249 individual scans which were used to generate imaging protocols for CT examinations.

Distribution by Age and Exposed Body Region

A detailed description of the cohort has been published elsewhere (*31*) and Fig. 4 provides complementary data on the distribution of the number of patients by age at first examination. Subjects exposed in mid-teen years (~15-year age group) and pre-teen years (5–10-year age groups) constituted the largest proportion of the cohort. As can be deduced by comparison of Figs. 4 and 5, some study subjects received more than one CT examination, with an overall average of approximately 1.5 CTs per subject. Details on the number of CT exams by body region are shown in Fig. 5. The predominant body part scanned was the head, representing, together with neck examinations, approximately 81% of all examinations. CT scans of the chest (13%) and abdomen/pelvis (9%) were the next most frequent examinations.

Primary Dose Findings

In this work, three summaries of estimated CT doses are presented, 1. organ dose per scan; 2. organ dose per examination; and 3. the overall distribution of individual cumulative organ doses, in the EPI-CT cohort subjects. Estimates of dose per scan are presented in the tables and are useful for describing the temporal pattern of typical organ doses to pediatric patients in the participating hospitals of nine European countries from single CT scans, beginning in the late 1970s until 2014. A summary of estimates of dose per examination, accounting for multiple scans per examination as explained above, are presented in the figures. Finally, a summary of the distribution of cumulative doses among the EPI-CT study subjects is
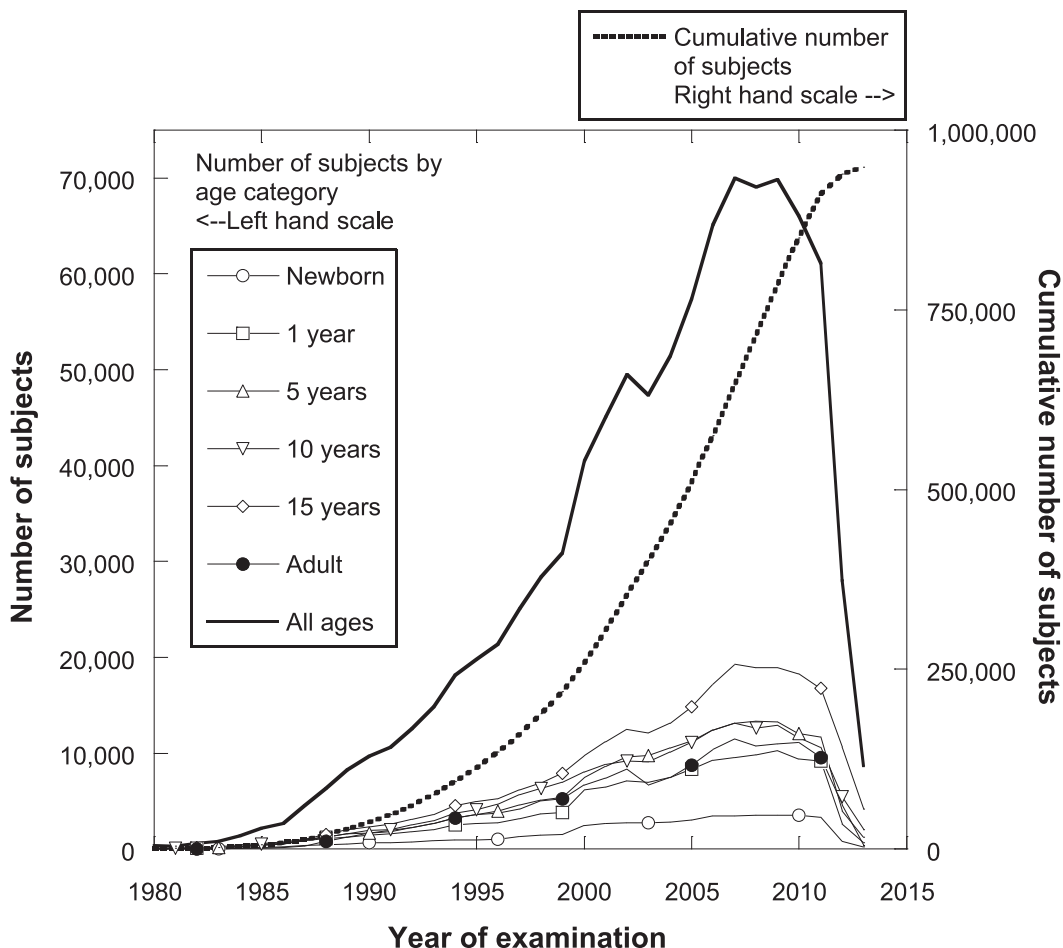
FIG. 4. Number of study subjects by age group [newborn (0 to 3 months of age), 1 year (4–30 months), 5 years (31–90 months), 10 years (91–150 months), 15 years (151–210 months) and adult (>210 months)] and examination year.

provided in the form of histograms and cumulative probability plots.

Whereas our dose reconstruction strategy is based on continuous introduction of new technology over time rather than on specific time periods, our findings are presented, for clarity, for three time periods (prior to 1991, from 1991 through 2000 and from 2001). The year 2001 should also not be viewed as an explicit beginning date for the use of pediatric protocols since the introduction of pediatric protocols in participating hospitals was simulated, as discussed above, in a smooth fashion with increasing proportion of hospitals using pediatric protocols over the period 1996 to 2006.

Tables 5–12 summarize estimated organ/tissue doses from scans of individuals for five target tissues (active bone marrow, brain, eye lens, thyroid and female breasts) by scan type (i.e., body region: head scan, chest scan, abdominal/pelvic scan). Since doses vary by body region scanned, there are three tables on dose for active bone marrow (head scan, chest scan, abdominal/pelvis scan) and two tables for dose to the thyroid gland (head scan and chest scan). Within each table, doses are summarized for the combination of the six age groups and the three time periods defined earlier so that both age-related and temporal changes can be observed.

The dose data presented in the tables on individual scans (as opposed to examinations) should be understood to represent statistical summaries of average organ-absorbed doses per scan for the number of persons in the subgroup described (e.g., newborn prior to 1991, newborn 1991–2000, newborn after 2001); i.e., they are the arithmetic average of the mean dose $(\overline{D}_{T,S})$ for each individual determined from 200 realizations. The variability of the estimated doses per scan among members of the defined group is represented by the 2.5 and 97.5 percentile values, standard deviation and coefficient of variation (CV) whereas the average individual uncertainty is presented as the group (age category and time period) average of the individual geometric standard deviation values (GSD)[7] where each GSD is determined for each subject from their

---

[7] Geometric standard deviation is used as a measure of dispersion of data in which logarithms are normally distributed (log-normal dispersion). The geometric standard deviation is calculated as the exponentiated value of the standard deviation of the log-transformed values.
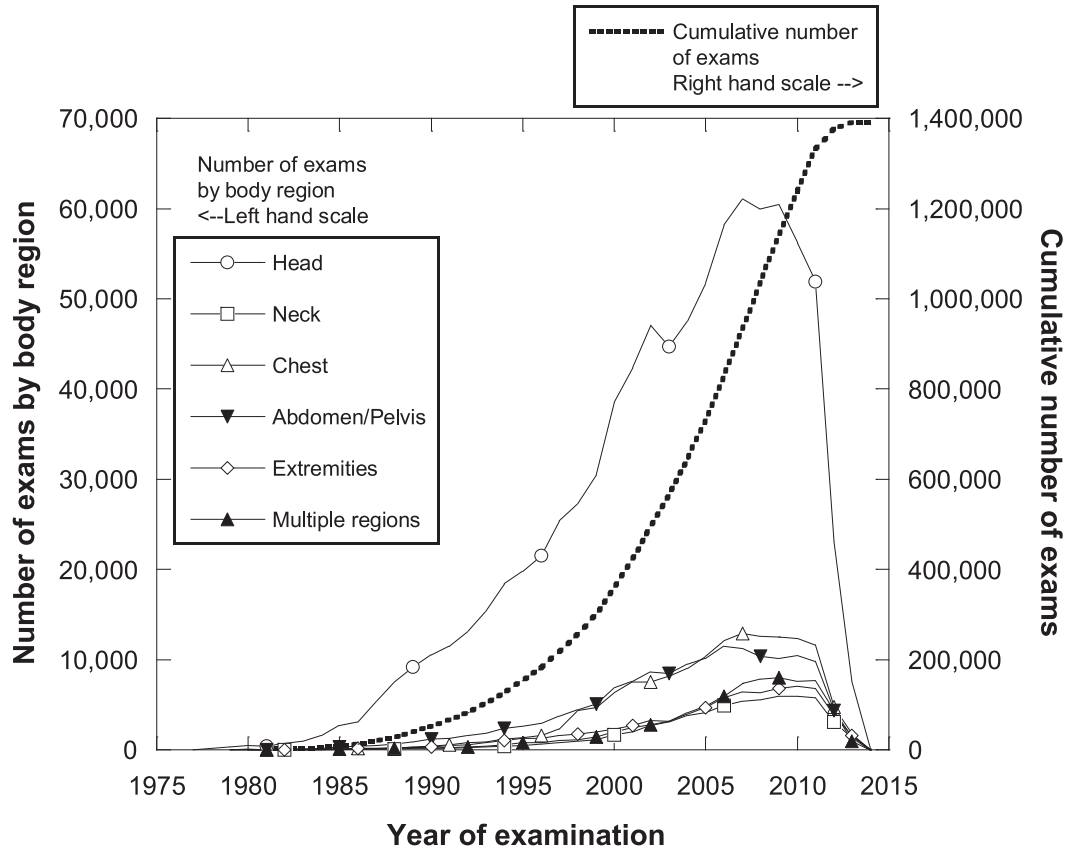
FIG. 5. Number of CT examinations by body region as a function of examination year.

TABLE 5
Summary Statistics on Mean Active Marrow Dose (mGy) from Single Head Scans to Six Age Groups [Newborn = 0–3 Months; 1 Year = 4–30 Months; 5 Years = 31–90 Months; 10 Years = 91–150 Months; 15 Years = 151–210 Months; Adults = >210 Months, for Three Time Periods (<1991, 1991–2000, and ≥2001)]

	<1991	1991–2000	≥2001	<1991	1991–2000	≥2001	<1991	1991–2000	≥2001
		Newborn			1 Year			5 Years	
N	3,160	12,448	31,551	7,896	35,049	101,124	8,911	43,372	124,962
Variation of arithmetic mean dose among sub-cohort members									
2.5–97.5%	9.7–20	10–25	5.9–20	9.4–20	7.9–25	5.3–21	6.1–17	5.4–21	4.4–19
Median	16	16	12	16	16	13	13	13	12
Mean	15	16	12	15	16	13	12	13	12
Standard deviation	2.6	4.0	4.0	2.8	4.2	4.1	3.0	4.0	4.0
Coefficient of variation (%)	17	25	32	18	26	32	25	32	34
Individual uncertainty from the 200 realizations									
Sub-cohort mean geometric standard deviation	1.9	2.0	2.3	1.9	2.0	2.3	2.0	2.0	2.4
		10 Years			15 Years			Adults	
N	8,984	47,085	113,738	9,994	49,767	151,585	3,840	33,743	88,904
Variation of arithmetic mean dose among sub-cohort members									
2.5–97.5%	3.6–11	3.0–12	2.2–13	2.0–6.6	2.0–7.5	1.2–7.1	0.91–4.0	1.1–4.4	0.71–4.3
Median	7.3	7.3	7.4	4.3	4.5	4.4	2.5	2.5	2.6
Mean	7.3	7.5	7.4	4.3	4.6	4.4	2.6	2.6	2.6
Standard deviation	2.0	2.5	2.8	1.2	1.4	1.5	0.7	0.8	0.9
Coefficient of variation (%)	28	34	38	28	31	35	27	32	35
Individual uncertainty from the 200 realizations									
Sub-cohort mean geometric standard deviation	1.9	1.9	2.4	1.9	1.9	2.2	1.9	2.0	2.2

TABLE 6
Summary Statistics on Mean Brain Dose (mGy) from Single Head Scans to Six Age Groups in Three Time Periods
(<1991, 1991–2000 and ≥2001)

	<1991	1991–2000 Newborn	≥2001	<1991	1991–2000 1 Year	≥2001	<1991	1991–2000 5 Years	≥2001
N	3,160	12,448	31,551	7,896	35,049	101,124	8,911	43,372	124,962
Variation of arithmetic mean dose among sub-cohort members									
2.5–97.5%	24–57	22–66	13–57	22–48	18–59	12–50	21–46	18–58	16–52
Median	46	44	34	39	38	32	37	37	35
Mean	45	44	35	37	39	32	36	37	35
Standard deviation	9.0	12	12	7.4	10	10	6.8	10	9.6
Coefficient of variation (%)	20	27	34	20	27	32	19	27	28
Individual uncertainty from the 200 realizations									
Sub-cohort mean geometric standard deviation	2.0	2.0	2.4	2.0	2.0	2.3	1.9	1.9	2.4
		10 Years			15 Years			Adults	
N	8,984	47,085	113,738	9,994	49,767	151,585	3,840	33,743	88,904
Variation of arithmetic mean dose among sub-cohort members									
2.5–97.5%	21–44	19–56	11–54	19–42	18–52	9.8–47	19–39	16–52	11–47
Median	37	37	37	34	36	35	33	34	33
Mean	35	36	36	33	35	33	32	34	32
Standard deviation	6.5	9.3	10	6.6	8.3	9.3	5.3	7.9	8.3
Coefficient of variation (%)	19	25	28	20	24	28	16	23	26
Individual uncertainty from the 200 realizations									
Sub-cohort mean geometric standard deviation	1.9	1.8	2.3	1.9	1.9	2.2	1.9	2.0	2.2

200 realizations. All doses in the tables are presented to two significant digits to represent the limits of the state of knowledge of the dose reconstruction.

Organ doses per scans. Organ dose data are presented in descending order of position in the body (from head to abdomen/pelvis). Here, ''mean dose'' refers to the arithmetic average of 200 realizations for an individual while ''sub-cohort mean'' refers to the arithmetic average of the mean doses for all subjects within the group described.

Table 5 presents summary data on active bone marrow dose from head scans. The mean active marrow dose per head scan ranged from 0.91 to 20 mGy before 1991 depending on the age, from 1.1 to 25 mGy for 1991–2000, and from 0.71 to 21 mGy after 2001. The sub-cohort mean dose per scan decreased over time by approximately 25% for the youngest ages and remained generally constant over time for adults. The variability, expressed by coefficient of variation, of the active marrow doses per head scan within a

TABLE 7
Summary Statistics on Mean Eye Lens Dose (mGy) from Single Head Scans to Six Age Groups in Three Time Periods
(<1991, 1991–2000 and ≥2001)

	<1991	1991–2000 Newborn	≥2001	<1991	1991–2000 1 Year	≥2001	<1991	1991–2000 5 Years	≥2001
N	3,160	12,448	31,551	7,896	35,049	101,124	8,911	43,372	124,962
Variation of arithmetic mean dose among sub-cohort members									
2.5–97.5%	28-59	32-79	22-62	25-52	28-70	22-57	25-53	28-71	24-63
Median	53	53	38	47	47	37	47	48	43
Mean	51	52	40	45	47	38	45	48	44
Standard deviation	8.1	12	12	6.9	11	9.9	7.0	11	9.9
Coefficient of variation (%)	16	23	29	15	23	26	15	24	22
Individual uncertainty from the 200 realizations									
Sub-cohort mean geometric standard deviation	1.9	1.9	2.3	1.9	1.9	2.3	1.9	1.9	2.3
		10 Years			15 Years			Adults	
N	8,984	47,085	113,738	9,994	49,767	151,585	3,840	33,743	88,904
Variation of arithmetic mean dose among sub-cohort members									
2.5–97.5%	24-51	27-66	16-64	25-52	29-70	15-62	25-49	22-67	18-64
Median	45	46	45	45	47	46	43	45	43
Mean	42	45	44	43	47	44	42	45	42
Standard deviation	7.1	10	10	7.2	9.8	11	5.6	9.8	9.9
Coefficient of variation (%)	17	23	24	17	21	24	14	22	24
Individual uncertainty from the 200 realizations									
Sub-cohort mean geometric standard deviation	1.9	1.8	2.3	1.9	1.9	2.1	1.9	1.9	2.1

THIERRY-CHEF *ET AL.*

TABLE 8
Summary Statistics on Mean Thyroid Dose (mGy) from Single Head Scans to Six Age Groups in Three Time Periods
(<1991, 1991–2000 and ≥2001)

	<1991	1991–2000 Newborn	≥2001	<1991	1991–2000 1 Year	≥2001	<1991	1991–2000 5 Years	≥2001
N	3,160	12,448	31,551	7,896	35,049	101,124	8,911	43,372	124,962
Variation of arithmetic mean dose among sub-cohort members									
2.5–97.5%	6.9–42	7.6–50	4.1–42	3.8–16	3.4–20	2.1–17	2.0–14	1.7–15	1.4–12
Median	22	23	20	9.1	9.2	7.2	7.6	7.5	6.7
Mean	22	24	20	9.4	10	8.3	7.7	7.8	6.6
Standard deviation	11	13	11	3.9	5.6	5.8	2.9	3.2	2.7
Coefficient of variation (%)	48	54	58	41	56	69	28	41	41
Individual uncertainty from the 200 realizations									
Sub-cohort mean geometric standard deviation	2.4	2.4	2.7	2.2	2.2	2.5	2.2	2.2	2.6
		10 Years			15 Years			Adults	
N	8,984	47,085	113,738	9,994	49,767	151,585	3,840	33,743	88,904
Variation of arithmetic mean dose among sub-cohort members									
2.5–97.5%	1.5–8.2	1.2–9.7	1.1–10	0.66–4.6	0.82–5.2	0.63–5.4	0.44–6.6	0.80–7.5	0.49–6.7
Median	6.2	6.1	6.5	3.1	3.2	3.3	3.1	3	2.8
Mean	5.8	5.9	5.9	3.0	3.1	3.2	3.4	3.3	3.1
Standard deviation	1.7	2.2	2.5	0.96	1.1	1.2	1.6	1.7	1.6
Coefficient of variation (%)	30	37	42	32	34	39	46	53	52
Individual uncertainty from the 200 realizations									
Sub-cohort mean geometric standard deviation	2.1	2.0	2.5	2.1	2.0	2.3	2.2	2.2	2.4

specific age group and time period was typically 20 to 40%. The same trend is seen for other organs in the head with the sub-cohort mean dose to the brain and lens of the eye decreasing over time by approximately 20% for the youngest ages (Tables 6 and 7, respectively).

Mean value of doses to the brain per head scan ranged from 19 to 57 mGy before 1991, depending on the age, from 16 to 66 mGy for 1991–2000, and from 9.8 to 57 mGy after 2001, with variability (CV) of mean brain doses per head scan, typically 20 to 30% (Table 6). As noted, variability was modest, particularly in the early years, reflecting relatively low adaptability of imaging protocols in head scans.

Doses to the eye lens (Table 7) were relatively high because of the shallow location of the eye lens and because the lens was assumed to be within the primary exposed

TABLE 9
Summary Statistics on Mean Thyroid Dose (mGy) from Single Chest Scans to Six Age Groups in Three Time Periods
(<1991, 1991–2000 and ≥2001)

	<1991	1991–2000 Newborn	≥2001	<1991	1991–2000 1 Year	≥2001	<1991	1991–2000 5 Years	≥2001
N	73	1,698	9,074	220	4,176	21,510	294	5,036	30,189
Variation of arithmetic mean dose among sub-cohort members									
2.5–97.5%	30–59	9.7–64	7.2–45	30–62	10–63	5.9–42	29–60	11–70	7.5–47
Median	49	30	13	50	30	11	49	40	14
Mean	48	34	18	49	34	16	45	40	19
Standard deviation	6.8	20	14	7.3	19	12	9.8	20	14
Coefficient of variation (%)	14	57	76	15	54	76	21	49	74
Individual uncertainty from the 200 realizations									
Sub-cohort mean geometric standard deviation	2.3	2.4	2.7	2.2	2.3	2.5	2.2	2.3	2.6
		10 Years			15 Years			Adults	
N	290	4,557	19,680	530	5,248	27,573	221	3,323	15,226
Variation of arithmetic mean dose among sub-cohort members									
2.5–97.5%	24–53	18–62	9.2–44	14–56	1.9–62	0.47–44	23–48	15–50	8.3–39
Median	41	36	18	36	34	21	39	32	22
Mean	38	37	21	35	34	22	37	31	22
Standard deviation	9.2	17	13	12	16	11	7.3	10	7.5
Coefficient of variation (%)	24	46	60	33	48	51	20	32	34
Individual uncertainty from the 200 realizations									
Sub-cohort mean geometric standard deviation	2.2	2.3	2.5	2.7	3.0	3.7	2.1	2.2	2.4

She

TABLE 10
Summary Statistics on Mean Female Breast Dose (mGy) from Single Chest Scans to Six Age Groups in Three Time Periods (<1991, 1991–2000 and ≥2001)

	<1991	1991–2000 Newborn	≥2001	<1991	1991–2000 1 Year	≥2001	<1991	1991–2000 5 Years	≥2001
N	34	671	3,763	95	1,699	8,889	133	2,208	13,711
Variation of arithmetic mean dose among sub-cohort members									
2.5–97.5%	25–52	8.6–58	6.1–39	21–43	7.6–44	4.1–30	18–40	7.3–45	4.8–30
Median	42	26	11	36	22	8.1	32	26	8.9
Mean	42	30	16	35	24	11	29	26	12
Standard deviation	5.6	18	13	5.1	12	8.4	6.6	13	8.8
Coefficient of variation (%)	13	60	80	14	49	75	22	50	72
Individual uncertainty from the 200 realizations									
Sub-cohort mean geometric standard deviation	2.2	2.3	2.7	2.2	2.3	2.5	2.2	2.3	2.6
		10 Years			15 Years			Adults	
N	140	2,119	9,134	251	2,411	12,230	81	1,330	6,765
Variation of arithmetic mean dose among sub-cohort members									
2.5–97.5%	15–34	11–41	6.1–28	14–31	10–36	7.6–26	16–33	12–39	11–28
Median	26	24	11	24	22	13	29	24	17
Mean	25	24	14	23	22	15	28	24	17
Standard deviation	5.6	11	8.4	5.2	7.7	5.5	4.1	7.6	4.7
Coefficient of variation (%)	22	46	60	23	35	37	15	32	27
Individual uncertainty from the 200 realizations									
Sub-cohort mean geometric standard deviation	2.1	2.3	2.5	2.1	2.2	2.4	2.1	2.2	2.3

region for all head scans (i.e., the exclusion of the eyes through gantry angulation was not simulated). Mean value of doses to the eye lens per head scan varied from 24 to 59 mGy before 1991, depending on the age, from 22 to 79 mGy for 1991–2000, and from 15 to 64 mGy after 2001. The variability (CV) of the mean eye lens doses per head scan was typically 15 to 30%.

Dose to the thyroid gland represents a more complex situation than for some other organs since it can potentially be exposed in head scans or in chest scans. The degree of exposure varies, depending on whether the scan slices include part or all of the thyroid gland or whether it is in close proximity to the scanned region. In the case of head scans, the thyroid gland is sometimes close to the inferior

TABLE 11
Summary Statistics on Mean Active Marrow Dose (mGy) from Single Chest Scans to Six Age Groups in Three Time Periods (<1991, 1991–2000 and ≥2001)

	<1991	1991–2000 Newborn	≥2001	<1991	1991–2000 1 Year	≥2001	<1991	1991–2000 5 Years	≥2001
N	73	1,698	9,074	220	4,176	21,510	294	5,036	30,189
Variation of arithmetic mean dose among sub-cohort members									
2.5–97.5%	12–23	3.7–25	2.6–17	9.5–19	3.5–20	1.7–14	5.7–14	2.5–15	1.4–10
Median	19	12	4.8	16	9.7	3.5	9.6	8.3	2.9
Mean	18	13	6.9	15	11	4.9	9.4	8.3	3.9
Standard deviation	2.6	7.6	5.3	2.4	6.0	3.9	2.4	4.2	3.0
Coefficient of variation (%)	14	57	77	15	55	78	25	50	76
Individual uncertainty from the 200 realizations									
Sub-cohort mean geometric standard deviation	2.2	2.4	2.7	2.2	2.4	2.5	2.2	2.3	2.6
		10 Years			15 Years			Adults	
N	290	4,557	19,680	530	5,248	27,573	221	3,323	15,226
Variation of arithmetic mean dose among sub-cohort members									
2.5–97.5%	5.3–11	3.9–13	1.9–9.5	4.9–11	3.7–13	2.2–9.1	4.8–12	3.5–12	3.1–9.5
Median	8.8	7.9	3.9	7.8	7.5	4.6	8.5	7.3	5.1
Mean	8.3	8.1	4.6	7.7	7.6	5.0	8.5	7.4	5.4
Standard deviation	1.9	3.7	2.8	2.0	3.0	2.0	1.9	2.5	1.6
Coefficient of variation (%)	23	46	61	25	40	41	22	34	30
Individual uncertainty from the 200 realizations									
Sub-cohort mean geometric standard deviation	2.1	2.3	2.5	2.1	2.2	2.5	2.1	2.2	2.3

TABLE 12
Summary Statistics on Mean Active Marrow Dose (mGy) from Single Abdominal/Pelvic Scans to Six Age Groups in Three Time Periods (<1991, 1991–2000 and ≥2001)

	<1991	1991–2000 Newborn	≥2001	<1991	1991–2000 1 Year	≥2001	<1991	1991–2000 5 Years	≥2001
N	147	727	2,025	430	2,684	8,118	673	4,646	13,571
Variation of arithmetic mean dose among sub-cohort members									
2.5–97.5%	4.1–18	2.9–14	1.1–11	4.3–15	3.6–14	1.0–11	3.8–13	3.5–12	1.4–9.7
Median	9.8	8.6	4.3	11	6.2	3.8	7.9	7.4	3.9
Mean	9.7	8.1	5.1	10	7.5	4.2	8.2	7.4	4.5
Standard deviation	3.6	3.4	3.0	3.2	3.5	2.5	2.5	2.5	2.3
Coefficient of variation (%)	37	42	59	31	47	60	30	34	52
Individual uncertainty from the 200 realizations									
Sub-cohort mean geometric standard deviation	2.1	2.2	2.7	2.1	2.2	2.6	2.1	2.2	2.6
		10 Years			15 Years			Adults	
N	805	6,866	19,890	1,505	9,771	40,741	842	8,163	29,340
Variation of arithmetic mean dose among sub-cohort members									
2.5–97.5%	4.5–15	4.1–13	2.4–11	4.3–14	4.3–13	3.4–12	5.4–14	4.2–12	2.9–11
Median	8.3	8.4	5.6	8.5	7.9	6.8	7.8	7	5.8
Mean	8.7	8.5	6.1	8.6	8.2	7.1	8.6	7.5	6.2
Standard deviation	2.6	2.5	2.6	2.4	2.3	2.3	2.4	2.3	2.2
Coefficient of variation (%)	30	29	44	28	29	32	28	31	36
Individual uncertainty from the 200 realizations									
Sub-cohort mean geometric standard deviation	2.1	2.2	2.5	2.0	2.2	2.4	2.1	2.1	2.3

boundary of the scan field. Table 8 summarizes doses to the thyroid gland per head scan. The mean value ranged from 0.44 to 42 mGy before 1991, depending on the age, from 0.80 to 50 mGy for 1991–2000, and from 0.49 to 42 mGy after 2001, with a decrease over time by 15% or less. The variability (CV) of mean thyroid doses per head scan was typically 40–70% with larger CVs reflecting the fact that the gland is usually outside the field for head scans.

The thyroid gland is almost always within the field for chest scans, thus, thyroid doses tended to be higher for chest scans compared to head scans in which the organ was rarely within the scan range (Table 9). Mean value of doses to the thyroid per chest scan ranged over all age groups from 14 to 62 mGy before 1991, from 1.9 to 70 mGy for 1991–2000, and from 0.47 to 47 mGy after 2001. Mean value of doses to the female breast per chest scan (Table 10) were generally slightly lower than doses to the thyroid. Doses vary over all age groups from 14 to 52 mGy before 1991, from 7.3 to 58 mGy for 1991–2000, and from 4.1 to 39 mGy after 2001.

Mean value of doses per scan to the active marrow from chest scans (Table 11) ranged from 4.8 mGy to 23 mGy before 1991, depending on the age, from 2.5 to 25 for 1991–2000, and from 1.4 to 17 mGy after 2001. In chest scans, the mean dose per scan for the three organs presented here decreased over time by more than 60% for the youngest ages and by approximately 40% for adults. The variability (CV) was typically 15 to 30% in the earliest time period but substantially increased (to approximately 70–80%) in later years for the youngest ages.

Mean value of doses per scan to active marrow from abdominal/pelvic scans ranged over all age groups from 3.8 to 18 mGy before 1991, from 2.9 to 14 mGy for 1991–

2000, and from 1.0 to 12 mGy after 2001 (Table 12). The mean dose decreased over time by approximately 50% for the youngest ages and approximately 30% for adults. The variability (CV) of mean active marrow doses per abdominal/pelvic scan was typically 30–60%.

Also shown in Tables 5 to 12 are sub-cohort mean values of the geometric standard deviation (GSD), each reflecting the uncertainty in individual doses. Whereas the sub-cohort mean GSD was typically of the order of 2, the upper mean GSD reached a value of 3.7 for thyroid doses in chest scans, which reflects higher uncertainty in dose for organs at the edge of the radiation field.

Organ doses per examinations. In contrast to estimates of doses per scan (Tables 5–12), Figs. 6 and 7 show data on doses per examination (Eq. 3), which account for multiple scans per examination. While most examinations were only a single scan, approximately 30% included more than one scan. As described earlier, the information on the number of scans per exam was unknown and, therefore, was treated as a stochastic variable in EPI-CT (Appendix 3; https://doi.org/ 10.1667/RADE-20-00231.1.S1). Figure 6 represents a summary of mean active marrow dose per examination after accounting for the uncertainty in the number of scans. Doses are presented by age category, by 5-year time periods, and by scanned body region. Analysis by 5-year time periods revealed a general trend with increasing doses between the 1980s and the 1990s. In general, the mean doses to active marrow from head examinations appeared to decrease afterward for the youngest two age categories, but there was little change at older ages. This pattern was also true for neck examinations. Compared to other organs, the decrease in dose to active marrow from chest scans was
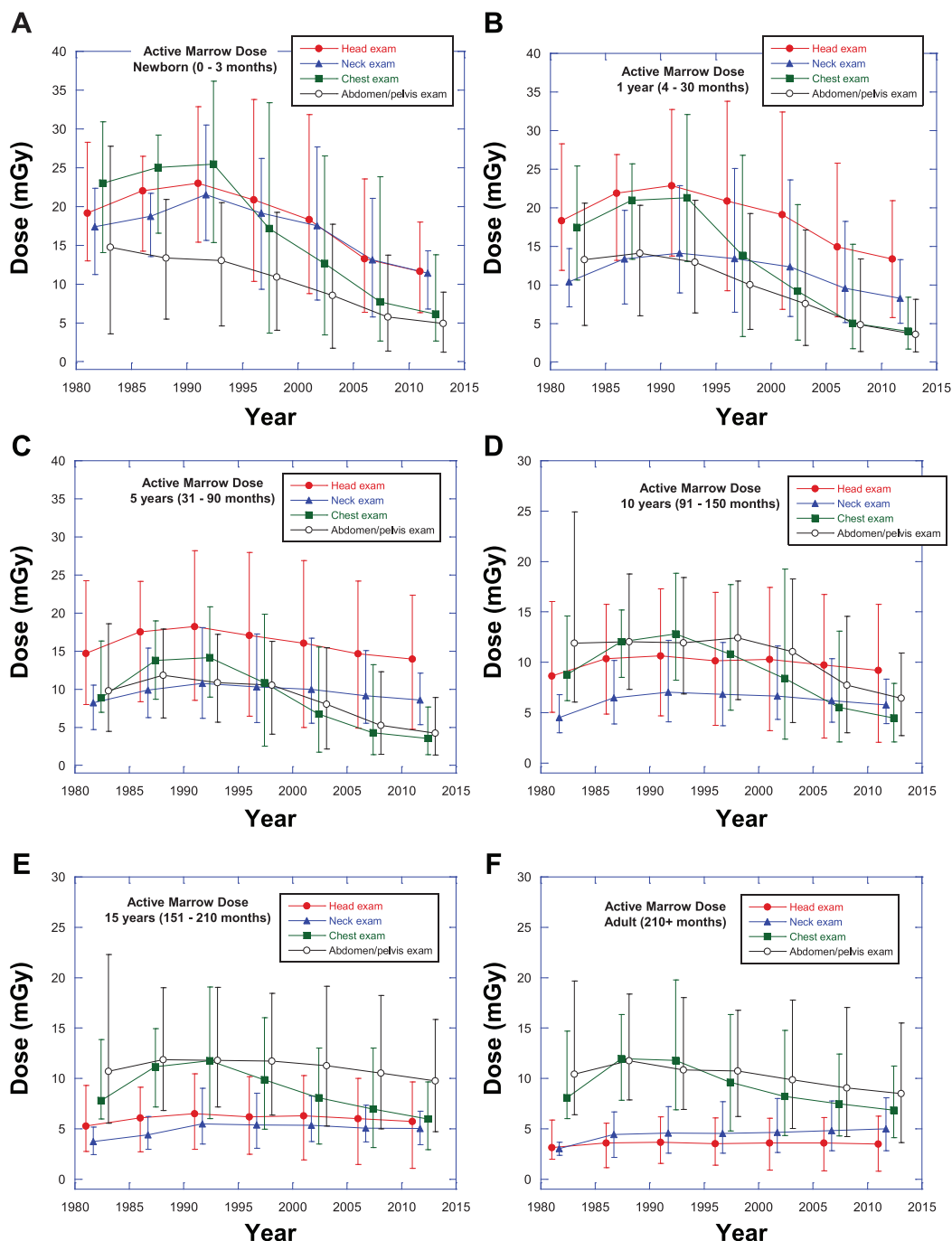
FIG. 6. Estimated mean active marrow doses (mGy) per examination by calendar year, body part (head, neck, chest and abdomen/pelvis) and age group. Panels A–F: Newborn (0–3 months age), 1 year (4–30 months age), 5 years (31–90 months age), 10 years (91–150 months age), 15 years (151–210 months age) and adult (>210 months age), respectively. Error bars are 95% ranges of individual mean dose estimates (average over 200 realizations). Y-axes differ according to panel.

larger at all ages. The magnitude of active marrow doses relative to each other within each age group reflects, in part, the evolution of the distribution of bone marrow in each part of the body with increasing age (Table 4). In all panels of Fig. 6, the first graphed point (1980s) had few data and, therefore, may not be completely representative for that year. Large error bars, reflecting variability of doses between examinations, are seen in the pediatric population for all body parts scanned; the variability is much less for head and neck scans in the adult population.

Figure 7 presents the brain, eye lens and thyroid dose from head examinations and thyroid dose from chest examinations by age category and time period. As shown, after the increase in doses in the 1980s–1990s, there was a
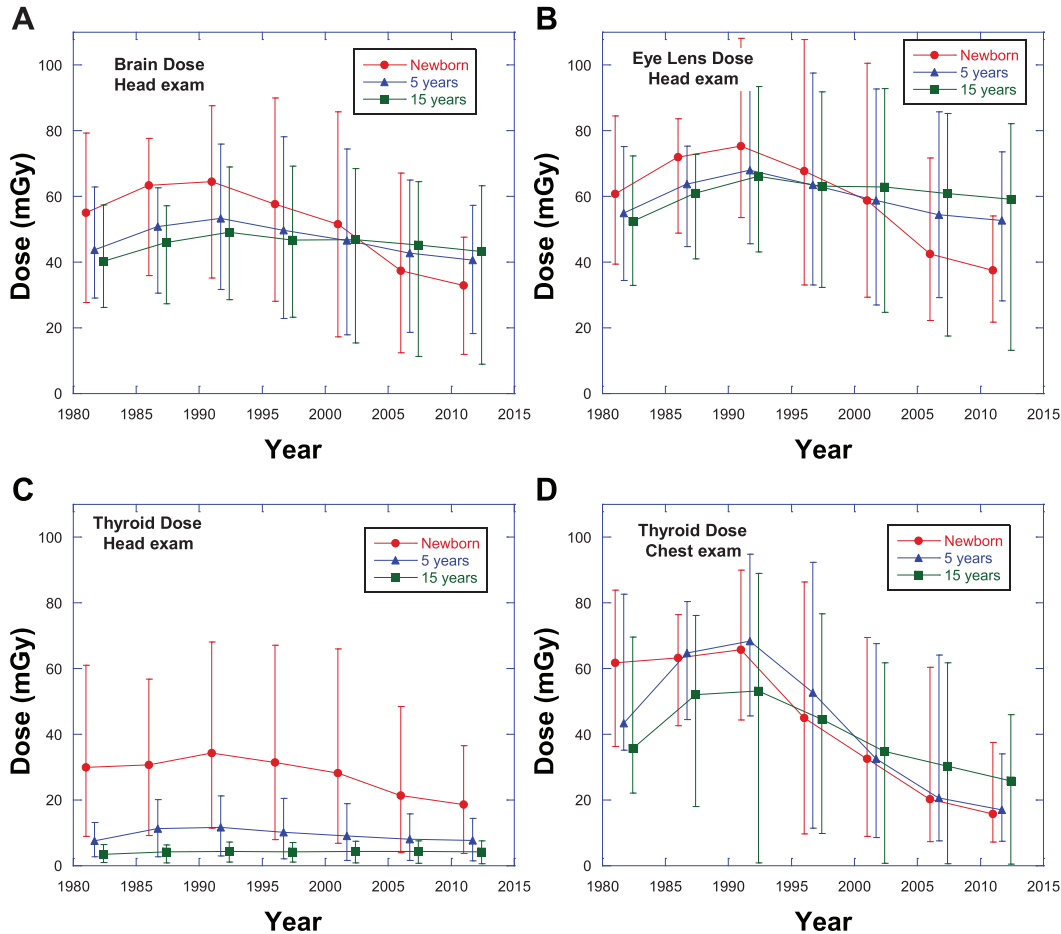
FIG. 7. Estimated sub-cohort mean doses (mGy) to the brain from head examinations (panel A), eye lens from head examinations (panel B), thyroid from head examinations (panel C), and thyroid from chest examinations (panel D) for a newborn (0–3 months age), a 5-year-old (31–90 months age) and 15-year-old (151–210 months age) subject. Error bars are 95% ranges of individual mean dose estimates (average over 200 realizations).

reduction by a factor of 2 of mean dose over time for brain and eye lens in younger patients (newborn) with the mean dose remaining nearly constant over time for older age groups. For all ages, brain and eye lens doses were comparable. Thyroid dose from chest scans was approximately twofold larger than thyroid dose from head examinations, almost exclusively because of the larger proportion of the thyroid gland that would be in the radiation field. Thyroid doses from head scans for the youngest age groups were larger in all time periods due to the closer proximity to the exposed region. Thyroid doses for head examinations decreased for younger patients and remained stable over time in older patients, whereas for chest examinations, a decrease was observed in all age groups.

Cumulative distribution functions of total doses per study subject. The final descriptive analysis to be presented in this work is a graphical summary of the total dose to the brain and to the active bone marrow for all members of the cohort from all scans each subject received, regardless of the body region scanned, based on the mean dose which describes the

200 realizations [Eq. (3)] for an individual. Figure 8A shows the cumulative distribution functions (CDFs) of the total doses received by the brain and active bone marrow of members of the cohort, by time period. The CDFs simply present the fraction of the cohort at any dose x that had doses less than or equal to that value. Figure 8B and C are two conventional frequency histograms of the data shown in the CDFs in Fig. 8A. Different information is conveyed by CDFs compared to frequency histograms; the combination of both methods demonstrates the range and frequency of doses received as well as the shapes of the distributions.

Figure 8 shows a decrease with time in the median brain dose, from about 58 mGy to 39 mGy, as well as a decrease in dose in all quantiles of the distribution. The figure also indicates that approximately 20% of the subjects received cumulative (total) doses to bone marrow of approximately 5 mGy or less, regardless of the time period. Another interesting feature is the multi-modal behavior of the brain dose. The CDFs (<1991, 1991–2000 and ≥2001) include all subjects in the cohort. This would, therefore, include scans to all body regions. The lowest doses are a result of
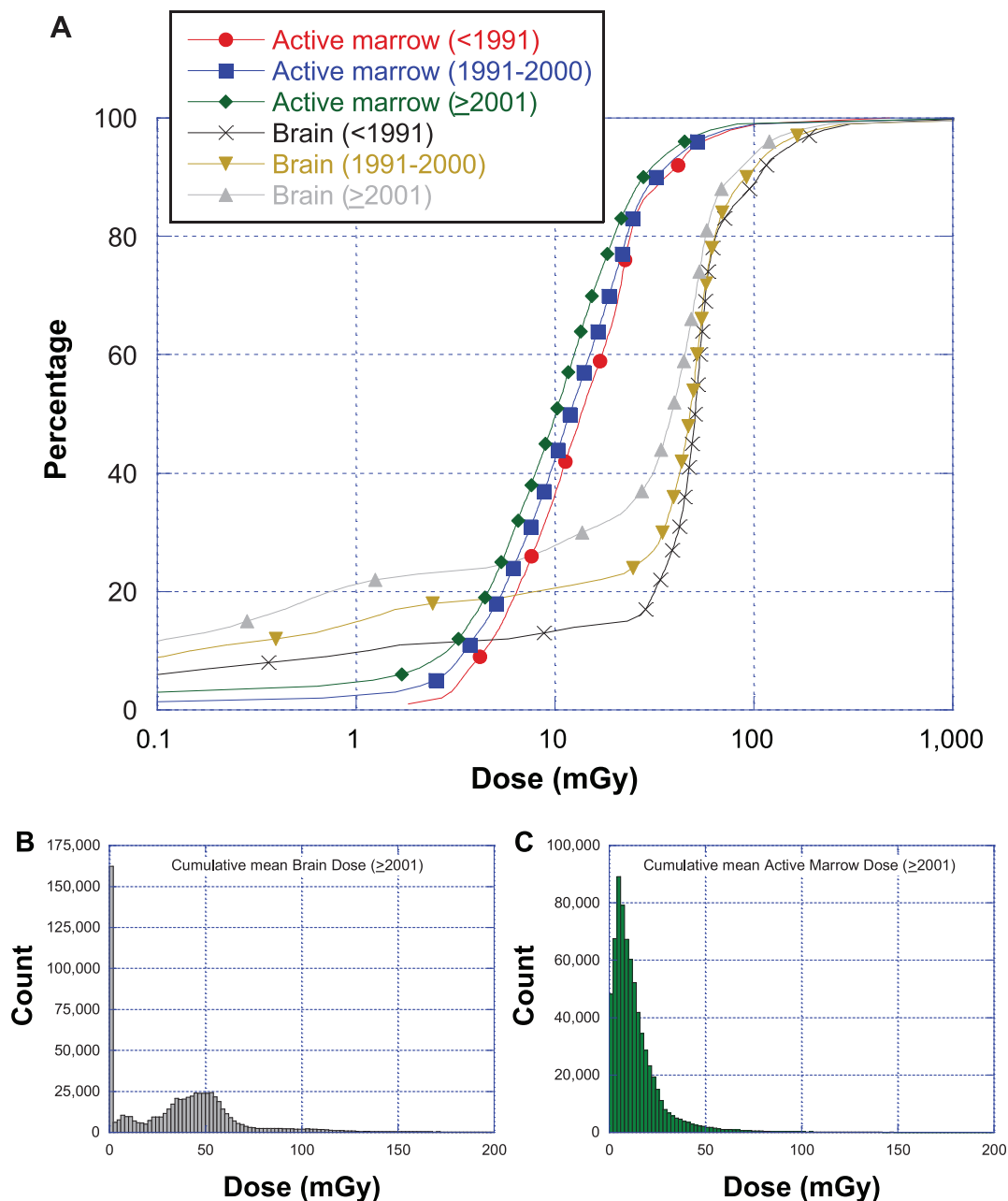
FIG. 8. Panel A: Cumulative distribution functions (CDFs) of total doses to the entire EPI-CT cohort before 1991, 1991–2000 and ≥2001 for brain and active bone marrow. Panels B and C: Frequency histograms of individual cumulative (total) brain dose and active marrow dose, respectively, for years ≥2001.

scans to body regions other than those at the edge of the head.

Internal Comparison

A direct comparison of the 2DMC doses was made with doses calculated from complete exposure parameters derived from PACS, using reliable one-to-one links between scans recorded in RIS and PACS (≈30,000 scans). For each single scan in this comparison, the median of the 200 simulated doses was divided by the point estimate dose

calculated from PACS data. The ratios ranged typically from about 0.1 to 10. Figure 9 shows histograms of the ratios for six groups selected by age, organ and examination type. The central tendency of the ratios is reasonably close to 1, giving confidence, on average, in the dose estimation of this study. The median of the ratios within each of these six groups ranges from 0.94 to 1.85. The mean of the ratios ranges from 1.45 to 3.29. These examples are typical, and highest values are based on a relatively low number of examinations. The comparison, as explained, supports the

Newborn and 1 year old
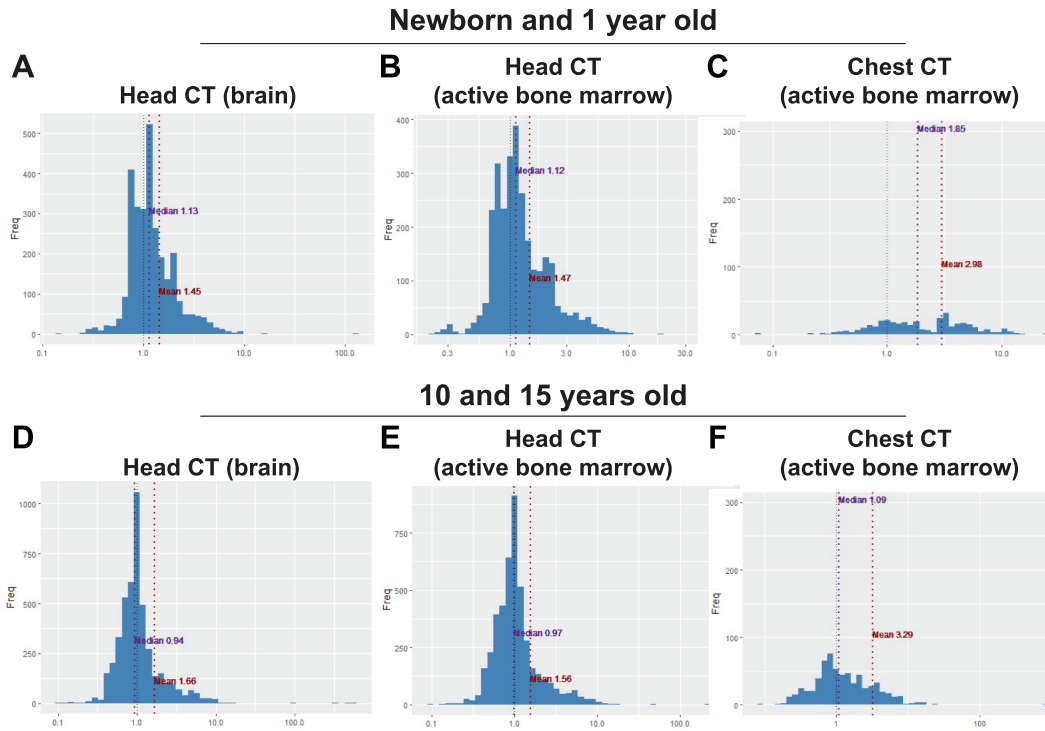
FIG. 9. Histograms of ratios between median dose from the 2DMC realizations and corresponding point doses (dotted lines) estimated using scan-specific PACS data. Panels A–C: Comparisons for CTs performed in the youngest patients (newborn and 1 year old), of brain doses for 2,902 head CTs (panel A), active bone marrow doses for the same 2,902 head CTs (panel B), and active marrow doses for 382 chest CTs (panel C). Panels D–F: Comparisons for CTs performed in patients in age groups 10 and 15 years, of brain doses for 4,495 head CTs (panel D), active bone marrow doses for the same 4,495 head CTs (panel E), and active marrow doses for 659 chest CTs (panel F).

validity of the dose reconstruction and the uncertainty assessment using the 2DMC method. On average within groups (by age, organ, examination type), the 2DMC doses were consistent with doses calculated when all exposure parameters were known.

Complementary comparison at the individual scan level was possible with the Dutch data, where a predictive model for dose was independently developed. As presented in Table 13, this subsequent analysis confirmed that doses from head scans, which represent the vast majority of examinations, derived in the Netherlands (*28*), and doses derived in EPI-CT, are on average very comparable (with slightly higher estimates in the Dutch study compared with our results) (Fig. 10). For other examination types, doses tended to be higher in our estimation compared to the national estimation. It should be noted that the number of examinations on which the comparison is based is sometimes limited (e.g., 77 lung high-resolution CTs in the Dutch data). Some of the difference may be due to the different anatomical landmarks considered in the two dose reconstruction systems, as the Dutch estimation of the exposed anatomical region tended to be systematically lower than our estimation. These comparisons, of course, do not confirm either dataset but, simply, point out some

differences which may be due to under- or overestimation by one or both methods.

DISCUSSION

The objective of the current work is to report on the methods used to reconstruct doses for 1,430,454 CT examinations performed over the years on a cohort of 948,174 children recruited in nine European countRies. The methods and tool were developed for the specific purpose of retrospective dose reconstruction and are not suitable for clinical predictions of doses to individual patients. Together with the description of the methods, the reader is provided with summary dose data which were reconstructed for the purpose of epidemiological investigation. Although the true organ dose to each study subject in the EPI-CT cohort cannot be precisely determined because of data limitations, we believe that significant advances and improvements over previously reported studies have been achieved, particularly in the area of estimation of uncertainty.

Individual Dose Estimates and Uncertainties

The dose reconstruction strategy implemented in the EPI-CT study is not intended to provide a single best estimate of

TABLE 13
Comparison of Sub-cohort Mean Doses per Scan from the Current Work and Previous Analyses

		EPI-CT		UK Study			Dutch Study	U.S. Study
Time period[a]	Age group	Dose per scan[b]	Dose per exam[b]	Kim *et al.* (67)[c]	Lee *et al.* (55)	Lee *et al.* (68)	Meulepas *et al.* (28)	Miglioretti *et al.* (20)
Head CT: Active marrow doses (mGy)								
<1990	All ages	2.6–15	3.5–21	1.3–16	16	11	17	
1990–2000	All ages	2.6–16	3.6–22	1.3–16	13	7	13	
≥2001	0–4	12–13	15–16	8–8.6	10	8	9	11
	5–10	7.4–12	10–15	6–8.6	9	6	8	6.5
	10–14	4.4–7.4	6.1–10	4.7–6	7	4	6	4.2
	15–19	2.6–4.4	3.6–6.1	2.1–4.4	5	2	5	
Head CT: Brain doses (mGy)								
<1990	All ages	32–45	44–62	32–56	62	52	52	
1990–2000	All ages	34–44	46–60	32–56	50	38	44	
≥2001	0–4	32–35	40–43	23–27	31	24	30	29
	5–10	35–36	44–47	28–35	33	24	30	25
	10–14	33–36	45–47	35–41	38	26	31	30
	15–19	32–33	44–45	37–42	33	29	31	
Abdomen/pelvis (or abdomen): Active marrow doses (mGy)								
<1990	All ages	8.2–10	12–15	4.3–7.6	9		6	
1990–2000	All ages	7.4–8.5	11–14	4.3–7.6	7		4	
≥2001	0–4	4.2–5.1	7.3–8.0	1.8–2.8	1		3	5.1
	5–10	4.5–6.1	6.8–9.4	1.6–2.8	5		3	5.6
	10–14	6.1–7.1	9.4–11	2.8	5		2	9.2
	15–19	6.2–7.1	9.8–11	2.8	4		2	

Note. Sub-cohort mean doses per examination from the current work are also provided for information.

[a] It should be noted that year 2000 was included in the latest period in the UK study.

[b] EPI-CT doses are reported as range of cohort mean organ doses (per scan or per examination) for the corresponding age groups: ''All ages'' includes the six age groups from our analysis; ''0–4'' includes newborn and 1-year age groups; ''5–10'' includes 5- and 10-year age groups; 10–15 includes 10- and 15-year age groups; and 15–19 includes 15-year and adult age groups.

[c] Data are provided for each year of age elsewhere [see (67)]. The range of doses provided here reflects the variability within each age category.

the organ dose for each individual scan, but rather, to provide a range of possible values of the dose for each scan. For the majority of examination types, organs, age groups and time periods, the uncertainty in individual doses was estimated by a geometric standard deviation of around 2 to 2.5, with a general trend of greater uncertainty in the later time period, which could be explained by the increased adaptability of CT protocols to individual patients in recent years. In fact, after an increase in doses between the 1980s and the 1990s resulting from the introduction of multi-slice CT scanners, concerns about CT exposures in the pediatric population have prompted scanner manufacturers to develop and implement options to appropriately manage and reduce the radiation dose (58, 59). The advances in technology include the following (60, 61):

1. Choice of a reference dose for a given image quality (effective mAs or noise index, for example).
2. Automatic tube current (mA) modulation (56, 57), which adapts tube current to thickness and density of scanned part of patient (for example, less mA for lungs, more mA for shoulders or pelvis). In our study, the use of PerMoS as software to extract data from the PACS allowed us to account for automatic exposure control as the value of mAs recorded is the average mAs value delivered.

3. Variation of tube potential (kV) based on body part thickness and density (some manufacturers). Tube current modulation (TCM) could not be considered in our analysis and the effect will be larger on superficial organs. The relative difference in organ dose conversion coefficients with and without TCM is for many organs and examinations less than 10%, but can in some cases amount up to 30%, e.g., for the thyroid in the chest CT (62).
4. Spectral CT, which is rarely used for children.

A further technological improvement is the replacement of filtered back projection (FBP) with iterative reconstruction, or model-based iterative reconstruction, which allows one to obtain the same image quality with less dose. This cannot be tuned to each individual patient, but the level of iterative reconstruction and the associated optional decrease in dose is embedded in the protocols (63).

Complementary to technological improvements, implementation of specific dose reduction techniques could have had a major impact on the actual doses received (64). In head scans, for example, if the eyes were fully excluded from the primary exposed region, e.g., due to gantry angulation, lens doses will have been substantially reduced. However, neither the individual use nor the frequency of use of such techniques could be evaluated in the framework
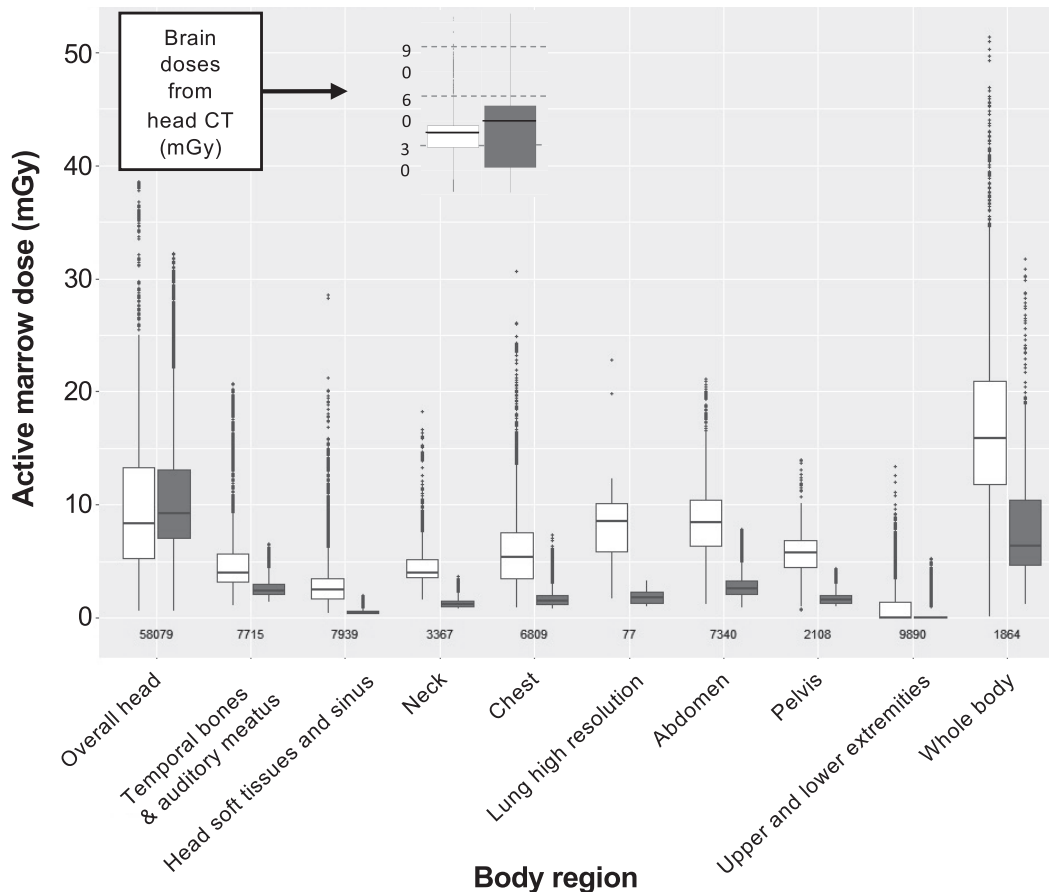
FIG. 10. Active marrow and brain doses per scans derived by body region with the EPI-CT dose reconstruction strategy (in white) compared with doses derived following the method implemented in the Netherlands (in black) (*28*).

of our study. A recently published study from the UK reported that more than one half of head scans included the lens within the primary exposed region (*65*). In Norway, 64% of the CT rooms participating in the 1991 survey reported tilted gantry parallel to the cranial vault, which reduced the lens doses considerably to give a mean dose of 3.9 (1.1–9.4) mGy (*37*). Gantry tilting could reduce dose to the eyes by up to 90% (*65, 66*).

More generally, the relative exposure of each organ is primarily determined by its location with respect to the body region that was scanned. The thyroid gland, for example, is almost always within the field for chest scans; therefore, thyroid doses tended to be higher for chest scans compared to head scans in which the organ is at the edge of the scan range (Fig. 7). Differences in doses to active bone marrow in each body region scanned are explained primarily by the differences in the proportion of active marrow in that region and secondarily by the photon fluence required to produce good diagnostic images. In general, for older patients, doses to active marrow from chest scans exceeded doses to active marrow from head scans because a larger proportion of the bone marrow is exposed in the chest, whereas the fraction of

bone marrow exposed in head and chest scans is comparable for younger patients (Table 4).

Comparison with Previously Published Dose Estimates

Our estimation of dose per scan compared well with organ doses published in the UK (*55, 67, 68*) (Table 13). These dose estimates utilize NCICT, although they are based on different data on exposure parameters. The agreement between doses estimated in the UK study and doses estimated in the EPI-CT study was confirmed when $CTDI_{vol}$ values were compared by examination type, time period and age (not shown) suggesting that the selection of machines and imaging protocols by the 2DMC agrees well with assumptions made in the UK study, especially in the early years. Comparison with doses published by others (*20, 28*) for recent years shows that our cohort mean doses per head scan (active marrow and brain doses) tend to be lower in early years whereas they tend to be higher in recent time periods. It should be noted that active marrow doses, as reported by Meulepas *et al*. (*28*), from abdominal/pelvic scans are also lower than our estimates in all time periods but they are in general lower than doses reported by others

(20, 55, 67, 68). Doses published for the French cohort of young children are also in good agreement with doses reported by others: mean brain and bone marrow dose for all examination types together are 23.1 and 8.9 mGy, respectively (21).

Strengths and Weaknesses

One of the most important attributes of dose estimation in the EPI-CT study is the derivation and application of a large number of imaging protocols (i.e., the combination of CT machine settings including kV, mAs, pitch, and choice of bowtie filter specific to age and body region scanned at a specific hospital), taking into account the renewal of CT machines with, in some hospitals, more than one CT room available at the same time period. The number of protocols employed in our study reached several tens of thousands. For comparison purposes, the UK study derived, from national surveys, a single typical protocol per body region prior to 2001, and four age group-related protocols for later years (67). The French study was based on 941 different protocols implemented in 23 pediatric hospitals between 2000 and 2010 (21). Dose estimations for the Dutch and Spanish cohorts were derived from the national PACS datasets, also included in our dataset (25, 28). Whereas in the Netherlands, a predictive model was derived from approximately 40,000 scans recorded in the PACS of 21 participating hospitals (28), in Spain, 17,000 CTs recorded in the PACS of nine Spanish hospitals were used to derive a lookup table of median and interquartile range of organ doses per examination type and 5-year age band (25).

An additional unique attribute of the EPI-CT cohort study is the integrated strategy for assessing and managing dosimetric uncertainty due to both uncertain but, also, missing parameters. Only in the UK has this been done to date (68). In the case of the EPI-CT study, with approximately 1 million patients and about 1.4 million scans, multiple realizations increased the data management requirements by 200-fold, making both management and quality assurance extremely challenging. Various graphical solutions for comparing realizations, e.g., the use of overlaid cumulative distribution function (52, 69), assisted considerably in determining whether the calculations were completed without data corruption or other obvious departures from reliable estimation.

We note that the sampling of the number of scans per examination, simulating possible unrecorded scans, is a unique feature of the EPI-CT dose reconstruction strategy as, to our knowledge, it has not been implemented elsewhere for the estimation of doses in epidemiological studies. Our dose per scan estimation compares well with previously published doses. We recommend, however, the use of dose per examination for subsequent risk analyses to account for scans which are not necessarily recorded in RIS.

While our dose estimations are based on the most comprehensive dataset available to date, numerous assumptions were required and, for that reason, our findings should be used with caution when evaluating doses in specific years in individual countries. We are aware that the main limitations in our assessment are associated with the observed variability in detailed information available for dose reconstruction by time period and by country. Whereas our dose estimation is based on a very large set of empirical data available for recent years, it is based on a relatively reduced number of protocol data to reflect the practice in the early years. Clearly, available data to reconstruct doses was less detailed for the early years and, therefore, for the cohorts with longer follow-up. Also, the main contributor to the study is the UK cohort for which only limited PACS data could be collected. As explained, our strategy aimed to overcome this limitation. Since there is no reason to anticipate major differences in practice among European countries, we believe that the use of the international dataset should provide reasonably good estimation overall.

An additional weakness is associated with the lack of data on body shape (height and weight) at the individual level combined with the use of the first version of the organ dose calculator (NCICT), which did not allow modification of the physical characteristics of the phantoms. A potential alternative approach, using the latest version of NCICT, which now allows height and weight to be selected, would be to sample these values for individual patients using national growth curves as PDFs. This approach would require obtaining historical growth curves to account for the two to three generations of patients in the cohort. This is considered to be a priority in anticipated further research.

Using the second version of NCICT, we were able to perform a sensitivity analysis to account for height and weight variability. We considered a 5-year-old male and a 5-year-old female with increasing height from 105 to 115 cm and increasing weight from 15 to 25 kg. Similarly, we considered two 15-year-old male and female, with height and weight varying from 155 cm and 40 kg to 185 (or 175) cm and 85 (or 75) kg, respectively, for male and female. Overall, for chest examination, dose to the lung varies by less than 20%, whereas dose to the colon in an abdominal CT could vary by 40% in older patients.

In addition to assessing the impact of body size and shape with potential for increased shielding by adipose tissue for larger patients (70), use of the upcoming version of the software will also allow for accounting of tube current modulation which can have substantial impact on organ doses with potential reduction by up to 40% (71–74).

Another limitation of our study is directly associated with the requirement to maintain confidentiality of patient data, preventing the collection of patient images. Therefore, we were unable to estimate, on an individual basis, the precise exposed body region and had to rely on expert judgement, which did not necessarily reflect the actual patient exposure conditions and could have introduced

uncertainty, particularly with respect to estimating the dose to organs at the edge of the field. Our strategy simulated random variation with respect to scan length among patients. Further analyses could potentially improve our estimation of exposed body region, assuming we had access to images on, at least, a sample of individual data undersigned informed consent. This is typically the information which should be available in a case-control study, such as the one implemented within the MEDIRAD project (http://www.medirad-project.eu/).

CONCLUDING REMARKS

In this EPI-CT study, organ doses from CT examinations were estimated in the largest cohort of CT-exposed individuals to date, comprised of approximately one million patients examined in nine European countries since the introduction of computed tomography in the late 1970s. Our dose reconstruction was designed for epidemiological evaluation and thus, the collected data do not necessarily represent full national coverage. For that reason, our doses are of limited use for national dose monitoring and are not presented by country. However, the temporal trends derived from our analysis reflect what we believe are real trends of CT doses over the years, with distinction between doses per scan, doses per examination and cumulative doses per individuals, especially when attention is given to the estimated uncertainties.

In addition to the size of the cohort, EPI-CT dosimetry is unique because of the calculation methodology implemented from PACS data for 437,249 individual scans used to derive PDFs of imaging protocols specific to patient age, body region examined, and time period, increasing the reliability and precision of the dose estimates to patients with known age, sex, and scanned body region over the conventional use of national survey data. The sex and age-resolution of phantoms (from newborn to adult) used for radiation dose estimates and the design of an integrated error propagation strategy are further important components. The dosimetry component of the EPI-CT study adds considerably to the knowledge on radiation exposures received by pediatric patients from CT examinations. We believe this study provides not just the largest set of reconstructed doses from CT to date, but the most detailed CT dose estimation for an epidemiological study conducted to date.

SUPPLEMENTARY INFORMATION

Appendix 1. EPI-CT dosimetry questionnaire.
Appendix 2. Doses to other organs. Summary statistics on mean doses (mGy) to various organs from head, chest, abdominal/pelvic or pelvic CT scans for the six age groups [i.e., newborn (0–3 months), 1 year (4–30 months), 5 years (31–90 months), 10 years (91–150 months), 15 years (151–

210 months), adults (>210 months)] and three time periods (<1991, 1991–2000, ≥2001):

Table A1. Mean salivary gland dose (mGy) from single head CT scans.
Table A2. Mean lung dose (mGy) from single chest CT scans.
Table A3. Mean esophageal dose (mGy) from single chest scans.
Table A4. Mean bladder dose (mGy) from single abdominal/pelvic CT scans.
Table A5. Mean colon dose (mGy) from single abdominal/pelvic CT scans.
Table A6. Mean kidney dose (mGy) from single abdominal/pelvic CT scans.
Table A7. Mean liver dose (mGy) from single abdominal/pelvic CT scans.
Table A8. Mean stomach dose (mGy) from single abdominal/pelvic CT scans.
Table A9. Mean ovarian dose (mGy) from single pelvic CT scans.
Table A10. Mean testes dose (mGy) from single pelvic CT scans.
Table A11. Mean skin dose (mGy) from single head CT scans.
Table A12. Mean skin dose (mGy) from single chest CT scans.
Table A13. Mean skin dose (mGy) from single abdominal/pelvic CT scans.
Appendix 3. PDFs of number of scans per examination for main examination types.

ACKNOWLEDGMENTS

REFERENCES

1. Medical radiation exposure of patients in the United States. NCRP report 184. Bethesda, MD: National Council on Radiation Protection and Measurements; 2019.

2. Report of the United Nations Scientific Committee on the Effects of Atomic Radiation. Volume 1 Annex A: Medical Radiation Exposures. New York: UNSCEAR; 2008.

3. Brenner DJ. We can do better than effective dose for estimating or comparing low-dose radiation risks. Ann ICRP 2012; 41:124–8.

4. Einstein AJ. Beyond the bombs: cancer risks of low-dose medical radiation. Lancet 2012; 380:455–7.

5. Kauffman JD, Litz CN, Thiel SA, Nguyen ATH, Carey A, Danielson PD, et al. To scan or not to scan: Overutilization of computed tomography for minor head injury at a pediatric trauma center. J Surg Res 2018; 232:164–70.

6. Brenner DJ, Hall EJ. Computed tomography–an increasing source of radiation exposure. N Engl J Med 2007; 357:2277–84.

7. Brenner D, Elliston C, Hall E, Berdon W. Estimated risks of radiation-induced fatal cancer from pediatric CT. AJR Am J Roentgenol 2001; 176:289–96.

8. Paterson A, Frush DP, Donnelly LF. Helical CT of the body: are settings adjusted for pediatric patients? AJR Am J Roentgenol 2001; 176:297–301.

9. McCollough CH, Zink FE. Performance evaluation of a multi-slice CT system. Med Phys 1999; 26:2223–30.

10. Giacomuzzi SM, Torbica P, Rieger M, Lottersberger C, Peer S, Peer R, et al. Radiation exposure in single slice and multi-slice spiral CT (a phantom study). (Article in German). ROFO Fortschr Geb Rontgenstr Nuklearmed 2001; 173:643–9.

11. Preston DL, Ron E, Tokuoka S, Funamoto S, Nishi N, Soda M, et al. Solid cancer incidence in atomic bomb survivors: 1958–1998. Radiat Res 2007; 168:1–64.

12. Akiba S, Mizuno S. The third analysis of cancer mortality among Japanese nuclear workers, 1991–2002: estimation of excess relative risk per radiation dose. J Radiol Prot Off J Soc Radiol Prot 2012; 32:73–83.

13. Grant EJ, Brenner A, Sugiyama H, Sakata R, Sadakane A, Utada M, et al. Solid cancer incidence among the Life Span Study of Atomic Bomb Survivors: 1958–2009. Radiat Res 2017; 187:513–37.

14. Committee to Assess Health Risks from Exposure to Low Levels of Ionizing Radiation. Health risks from exposure to low levels of ionizing radiation. BEIR VII Phase 2. Washington, DC: U.S. National Research Council; 2006.

15. High Level and Expert Group. High Level and Expert Group report on European low dose risk research-radiation protection. Report No. European Commission EUR 23884. Brussels: European Union; 2009.

16. Valentin J. Low-dose extrapolation of radiation-related cancer risk. ICRP Publication 99. Ann ICRP 35; 2005.

17. Berrington de Gonzalez A, Mahesh M, Kim K-P, Bhargavan M, Lewis R, Mettler F, et al. Projected cancer risks from computed tomographic scans performed in the United States in 2007. Arch Intern Med 2009; 169:2071–7.

18. Berrington de Gonzalez A, Salotti JA, McHugh K, Little MP, Harbron RW, Lee C, et al. Relationship between paediatric CT scans and subsequent risk of leukaemia and brain tumours: assessment of the impact of underlying conditions. Br J Cancer 2016; 114:388–94.

19. Pokora R, Krille L, Dreger S, Lee C, Günster C, Zeeb H, et al. Computed tomography in Germany. Dtsch Arzteblatt Int 2016; 113:721–8.

20. Miglioretti DL, Johnson E, Williams A, Greenlee RT, Weinmann S, Solberg LI, et al. The use of computed tomography in pediatrics and the associated radiation exposure and estimated cancer risk. JAMA Pediatr 2013; 167:700–7.

21. Journy N, Rehel J-L, Ducou Le Pointe H, Lee C, Brisse H, Chateil J-F, et al. Are the studies on cancer risk from CT scans biased by indication? Elements of answer from a large-scale cohort study in France. Br J Cancer 2015; 112:185–93.

22. Krille L, Dreger S, Schindel R, Albrecht T, Asmussen M, Barkhausen J, et al. Risk of cancer incidence before the age of 15 years after exposure to ionising radiation from computed tomography: results from a German cohort study. Radiat Environ Biophys 2015; 54:1–12.

23. Mathews JD, Forsythe AV, Brady Z, Butler MW, Goergen SK, Byrnes GB, et al. Cancer risk in 680,000 people exposed to computed tomography scans in childhood or adolescence: data linkage study of 11 million Australians. BMJ 2013; 346:f2360.

24. Pearce MS, Salotti JA, Little MP, McHugh K, Lee C, Kim KP, et al. Radiation exposure from CT scans in childhood and subsequent risk of leukaemia and brain tumours: a retrospective cohort study. Lancet Lond Engl 2012; 380:499–505.

25. Bosch de Basea M, Morina D, Figuerola J, Barber I, Muchart J, Lee C, et al. Subtle excess in lifetime cancer risk related to CT scanning in Spanish young people. Environ Int 2018; 120:1–10.

26. Huang W-Y, Muo C-H, Lin C-Y, Jen Y-M, Yang M-H, Lin J-C, et al. Paediatric head CT scan and subsequent risk of malignancy and benign brain tumour: a nation-wide population-based cohort study. Br J Cancer 2014; 110:2354–60.

27. Journy NMY, Lee C, Harbron RW, McHugh K, Pearce MS, Berrington de Gonzalez A. Projected cancer risks potentially related to past, current, and future practices in paediatric CT in the United Kingdom, 1990–2020. Br J Cancer 2017; 116:109–16.

28. Meulepas JM, Ronckers CM, Smets AMJB, Nievelstein RAJ, Gradowska P, Lee C, et al. Radiation exposure from pediatric CT scans and subsequent cancer risk in the Netherlands. J Natl Cancer Inst 2019; 111:256–63.

29. Berrington de Gonzalez A, Journy N, Lee C, Morton LM, Harbron RW, Stewart DR, et al. No association between radiation dose from pediatric CT scans and risk of subsequent Hodgkin lymphoma. Cancer Epidemiol Biomark Prev 2017; 26:804–6.

30. Bosch de Basea M, Pearce MS, Kesminiene A, Bernier M-O, Dabin J, Engels H, et al. EPI-CT: design, challenges and epidemiological methods of an international study on cancer risk after paediatric and young adult CT. J Radiol Prot Off J Soc Radiol Prot 2015; 35:611–28.

31. Bernier M-O, Baysson H, Pearce MS, Moissonnier M, Cardis E, Hauptmann M, et al. Cohort profile: the EPI-CT study: A European pooled epidemiological study to quantify the risk of radiation-induced cancer from paediatric CT. Int J Epidemiol 2019; 48:379–81g.

32. Olerud HM, Toft B, Flatabo S, Jahnen A, Lee C, Thierry-Chef I. Reconstruction of paediatric organ doses from axial CT scans performed in the 1990s – range of doses as input to uncertainty estimates. Eur Radiol 2016; 26:3026–33.

33. Journy NMY, Dreuil S, Boddaert N, Chateil J-F, Defez D, Ducou-le-Pointe H, et al. Individual radiation exposure from computed tomography: a survey of paediatric practice in French university hospitals, 2010–2013. Eur Radiol 2018; 28:630–41.

34. Jahnen A, Kohler S, Hermen J, Tack D, Back C. Automatic computed tomography patient dose calculation using DICOM header metadata. Radiat Prot Dosimetry 2011; 147:317–20.

35. Jacob P, Meckbach R, Kaiser JC, Sokolnikov M. Possible expressions of radiation-induced genomic instability, bystander effects or low-dose hypersensitivity in cancer epidemiology. Mutat Res 2010; 687:34–9.

36. Shrimpton PC, Jones DG, Hillier MC, Wall BF, Le Heron JC, Faulkner K. Survey of CT practice in the UK. Part 2. Dosimetric aspect report NRPB-R249. Chilton: National Radiological Protection Board; 1991.

37. Olerud HM. Analysis of factors influencing patient doses from CT in Norway. Radiat Prot Dosim 1997; 71:123–33.

38. Lee C, Kim KP, Bolch WE, Moroz BE, Folio L. NCICT: a computational solution to estimate organ doses for pediatric and adult patients undergoing CT scans. J Radiol Prot 2015; 35:891–909.

39. Lee C, Kim KP, Long DJ, Bolch WE. Organ doses for reference pediatric and adolescent patients undergoing computed tomography estimated by Monte Carlo simulation. Med Phys 2012; 39:2129–46.

40. Lee C, Lodwick D, Hurtado J, Pafundi D, Williams JL, Bolch WE. The UF family of reference hybrid phantoms for computational radiation dosimetry. Phys Med Biol 2010; 55:339–63.

41. Thierry-Chef I, Dabin J, Friberg EG, Hermen J, Istad TS, Jahnen A, et al. Assessing organ doses from paediatric CT scans–a novel approach for an epidemiology study (the EPI-CT study). Int J Environ Res Public Health 2013; 10:717–28.

42. Bolch WE, Eckerman K, Endo A, Hunt JGS, Jokisch DW, Kim CH, et al. ICRP Publication 143: Paediatric reference computational phantoms Ann ICRP 2020; 49:5–297.

43. Menzel HG, Clement C, DeLuca P. ICRP Publication 110. Realistic reference phantoms: an ICRP/ICRU joint effort. A report of adult reference computational phantoms. Ann ICRP 2009; 39:1–164. Erratum in: Ann ICRP 2009; 39:165.

44. Stamm G, Nagel HD. CT-expo–a novel program for dose evaluation in CT. (Article in German). ROFO Fortschr Geb Rontgenstr Nuklearmed 2002; 174:1570–6.

45. impactscan.org. ImPact's ct dosimetry tool. (http://www.impactscan.org/ctdosimetry.htm)

46. Cristy M. Mathematical phantoms representing children of various ages for use in estimates of internal dose. Report No. NUREG/CR-1159; ORNL/NUREG/TM-367. Oak Ridge, TN: Oak Ridge National Lab; 1980. (https://bit.ly/3mddMPH)

47. Dabin J, Mencarelli A, McMillan D, Romanyukha A, Struelens L, Lee C. Validation of calculation algorithms for organ doses in CT by measurements on a 5 year old paediatric phantom. Phys Med Biol 2016; 61:4168–82.

48. Tian X, Li X, Segars WP, Frush DP, Paulson EK, Samei E. Dose coefficients in pediatric and adult abdominopelvic CT based on 100 patient models. Phys Med Biol 2013; 58:8755–68.

49. Turner AC, Zhang D, Khatonabadi M, Zankl M, DeMarco JJ, Cagnon CH, et al. The feasibility of patient size-corrected, scanner-independent organ dose estimates for abdominal CT exams. Med Phys 2011; 38:820–9.

50. Report of the United Nations Scientific Committee on the effects of Atomic Radiation. Volume II Annex B: Effects of radiation exposure of children. New York: UNSCEAR; 2013.

51. Ainsbury EA, Bouffler SD, Dorr W, Graw J, Muirhead CR, Edwards AA, et al. Radiation cataractogenesis: a review of recent studies. Radiat Res 2009; 172:1–9.

52. Simon SL, Hoffman FO, Hofer E. The two-dimensional Monte Carlo: a new methodologic paradigm for dose reconstruction for epidemiological studies. Radiat Res 2015; 183:27–41.

53. European Commission Radiation Protection. European guidance on estimating population doses from medical X-ray procedures. Report No. 154. Brussels: European Commission; 2008.

54. European Commission Radiation Protection. Medical radiation exposure of the European population. Report No. RP180 1/2, Brussels: European Commission; 2014.

55. Lee C, Pearce MS, Salotti JA, Harbron RW, Little MP, McHugh K, et al. Reduction in radiation doses from paediatric CT scans in Great Britain. Br J Radiol 2016; 89:20150305.

56. Gies M, Kalender WA, Wolf H, Suess C. Dose reduction in CT by anatomically adapted tube current modulation. I. Simulation studies. Med Phys 1999; 26:2235–47.

57. Kalender WA, Wolf H, Suess C. Dose reduction in CT by anatomically adapted tube current modulation. II. Phantom measurements. Med Phys 1999; 26:2248–53.

58. Huda W, Bushong SC. In x-ray computed tomography, technique factors should be selected appropriate to patient size. Med Phys 2001; 28:1543–5.

59. McCollough CH, Bruesewitz MR, Kofler JM. CT dose reduction and dose management tools: overview of available options. Radiographics 2006; 26:503–12.

60. Goo HW. CT radiation dose optimization and estimation: an update for radiologists. Korean J Radiol 2012; 13:1–11.

61. Kaza RK, Platt JF, Goodsitt MM, Al-Hawary MM, Maturen KE, Wasnik AP, et al. Emerging techniques for dose optimization in abdominal CT. Radiographics 2014; 34:4–17.

62. Schlattl H, Zankl M, Becker J, Hoeschen C. Dose conversion coefficients for paediatric CT examinations with automatic tube current modulation. Phys Med Biol 2012; 57:6309–26.

63. Silva AC, Lawder HJ, Hara A, Kujak J, Pavlicek W. Innovations in CT dose reduction strategy: application of the adaptive statistical iterative reconstruction algorithm. AJR Am J Roentgenol 2010; 194:191–9.

64. Malchair F, Maccia C. Practical advice for optimal CT scanner dose in children. Radioprotection 2020; 55:117–22.

65. Harbron RW, Ainsbury EA, Barnard SGR, Lee C, McHugh K, Berrington de Gonzalez A, et al. Radiation dose to the lens from CT of the head in young people. Clin Radiol 2019; 74:816.e9–17.

66. Lai C-K, Cheung H-Y, Chan T-P, Wong T. Reducing the radiation dose to the eye lens region during CT brain examination: the potential beneficial effect of the combined use of bolus and a bismuth shield. Radioprotection 2015; 50:195–201.

67. Kim KP, Berrington de Gonzalez A, Pearce MS, Salotti JA, Parker

L, McHugh K, et al. Development of a database of organ doses for paediatric and young adult CT scans in the United Kingdom. Radiat Prot Dosimetry 2012; 150:415–26.

68. Lee C, Journy N, Moroz BE, Little M, Harbron R, McHugh K, et al. Organ dose estimation accounting for uncertainty for pediatric and young adult CT scans in The United Kingdom. Radiat Prot Dosimetry 2019; 184:44–53.

69. Land CE, Kwon D, Hoffman FO, Moroz B, Drozdovitch V, Bouville A, et al. Accounting for shared and unshared dosimetric uncertainties in the dose response for ultrasound-detected thyroid nodules after exposure to radioactive fallout. Radiat Res 2015; 183:159–73.

70. Lee C, Flynn MJ, Judy PF, Cody DD, Bolch WE and Kruger RL. Body size–specific organ and effective doses of chest CT screening examinations of the National Lung Screening Trial. AJR Am J Roentgenol 2017; 208:1082–8.

71. Zacharia TT, Kanekar SG, Nguyen DT, Moser K. Optimization of patient dose and image quality with z-axis dose modulation for computed tomography (CT) head in acute head trauma and stroke. Emerg Radiol 2011; 18:103–7.

72. Papadakis AE, Damilakis J. Automatic tube current modulation and tube voltage selection in pediatric computed tomography. Invest Radiol 2019; 54:265–72.

73. Li X, Segars WP, Samei E. The impact on CT dose of the variability in tube current modulation technology: A theoretical investigation. Phys Med Biol 2014; 59:4525–48.

74. McMillan K, Bostani M, Cagnon CH, Yu L, Leng S, McCollough CH, et al. Estimating patient dose from CT exams that use automatic exposure control: Development and validation of methods to accurately estimate tube current values. Med Phys 2017; 44:4262–75.